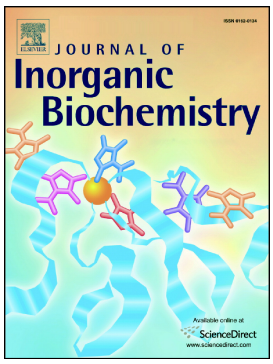

Chemistry of mixed-ligand oxidovanadium(IV) complexes of aroylhydrazones incorporating quinoline derivatives: Study of solution behavior, theoretical evaluation and protein/DNA interaction

Atanu Banerjee, Subhashree P. Dash, Monalisa Mohanty, Daniele Sanna, Giuseppe Sciortino, Valeria Ugone, Eugenio Garribba, Hans Reuter, Werner Kaminsky, Rupam Dinda

PII: S0162-0134(19)30269-7
DOI: https://doi.org/10.1016/j.jinorgbio.2019.110786
Article Number: 110786
Reference: JIB 110786

To appear in: *Journal of Inorganic Biochemistry*

Received date: 6 May 2019
Revised date: 15 July 2019
Accepted date: 16 July 2019

Please cite this article as: A. Banerjee, S.P. Dash, M. Mohanty, et al., Chemistry of mixed-ligand oxidovanadium(IV) complexes of aroylhydrazones incorporating quinoline derivatives: Study of solution behavior, theoretical evaluation and protein/DNA interaction, Journal of Inorganic Biochemistry, https://doi.org/10.1016/j.jinorgbio.2019.110786

Chemistry of mixed-ligand oxidovanadium(IV) complexes of aroylhydrazones incorporating quinoline derivatives: Study of solution behavior, theoretical evaluation and protein/DNA interaction

Atanu Banerjee,[a] Subhashree P. Dash,[a,b] Monalisa Mohanty,[a] Daniele Sanna,[c] Giuseppe Sciortino,[d,e] Valeria Ugone,[e] Eugenio Garribba,*[,e] Hans Reuter,[f] Werner Kaminsky,[g] Rupam Dinda*[,a]

[a]*Department of Chemistry, National Institute of Technology, Rourkela, 769008 Odisha, India. E-mail: rupamdinda.nitrkl@gmail.com.*

[b]*Department of Basic Sciences, Parala Maharaja Engineering College, Sitalapalli, Brahmapur, Odisha 761003, India*

[c]*Istituto CNR di Chimica Biomolecolare, Trav. La Crucca 3, I-07040 Sassari, Italy.*

[d]*Departament de Química, Universitat Autònoma de Barcelona, 08193 Cerdanyola del Vallés, Barcelona, Spain.*

[e]*Dipartimento di Chimica e Farmacia, Università di Sassari, Via Vienna 2, I-07100 Sassari, Italy. E-mail: garribba@uniss.it.*

[f]*Institute of Chemistry of New Materials, University of Osnabrück, Barbarastraße 6, 49069 Osnabruck, Germany.*

[g]*Department of Chemistry, University of Washington, Seattle, Washington 98195, United States*

Abstract

A series of eight hexacoordinated mixed-ligand oxidovanadium(IV) complexes [VO($\mathbf{L}^{x}$)($\mathbf{L}^{N-N}$)] (**1-8**), where $\mathbf{L}^{x}$ = $\mathbf{L}^{1}$ – $\mathbf{L}^{4}$, are four differently substituted ONO donor aroylhydrazone ligands and $\mathbf{L}^{N-N}$ are *N,N*-donor bases like 2,2′-bipyridine (bipy) (**1**, **3**, **5** and **7**) and 1,10-phenanthroline (phen) (**2**, **4**, **6** and **8**) have been reported. All synthesized complexes have been characterized by various physicochemical techniques and molecular structures of **1** and **6** were determined by X–ray crystallography. With a view to evaluate the biological activity of the $V^{IV}O$ species, the behavior of the systems $V^{IV}O^{2+}/\mathbf{L}^{x}$, $V^{IV}O^{2+}/\mathbf{L}^{x}$/bipy and $V^{IV}O^{2+}/\mathbf{L}^{x}$/phen was studied as a function of pH in a mixture of H_2O/DMSO 50/50 (v/v). DFT calculations allowed finding out the relative stability of the tautomeric forms of the ligands, and predicting the structure of vanadium complexes and their EPR parameters. To study their interaction with proteins, firstly the ternary systems $V^{IV}O^{2+}/\mathbf{L}^{1,2}$ with 1-methylimidazole, which is a good model for histidine binding, were examined. Subsequently the interaction of the complexes with lysozyme (Lyz), cytochrome *c* (Cyt) and bovine serum albumin (BSA) was studied. The results indicate that the complexes showed moderate binding affinity towards BSA, while no interaction takes place with lysozyme and cytochrome *c*. This could be explained with the higher number of accessible coordinating and polar residues for BSA than for Lyz and Cyt. Further, the complexes were also evaluated for their DNA binding propensity through UV-vis absorption titration and fluorescence spectral studies. These results were consistent with BSA binding affinity and showed moderate binding affinity towards CT-DNA.

Keywords: Aroylhydrazone/ mixed-ligand oxidovanadium(IV)/ protein interaction/ DNA binding/ DFT Calculation.

1. Introduction

Among the transition metals, the chemistry of vanadium and its complexes has become a fascinating area of research after the discovery of vanadium as a bio-essential element and its presence in many naturally occurring compounds [1,2]. It has stimulatory effect on the growth of algae and plants [3], participating in various enzymatic reactions like, the inhibitory action of vanadate(V) on Na, K-ATPase [4], haloperoxidases [5] and some nitrogenases in nitrogen-fixing *Azotobacter* [6,7].

Vanadium compounds also show a wide variety of pharmacological properties like anti parasitic, spermicidal, anti-viral, anti- HIV, anti-tuberculosis and anti-tumor activity [8-14]. In the last 20 years, the anti-diabetic activity of vanadium complexes has been widely investigated [15]. Due to its insulin like effect, vanadium complexes have been extensively studied for their potential use in the treatment of type II diabetes mellitus [16-21]. Among these compounds, bis(maltolato)oxidovanadium(IV) (BMOV) has become the standard complex for the new vanadium-based molecules with antidiabetic action [22,23], while its derivative bis(ethylmaltolato)oxidovanadium-(IV) (BEOV) has entered phase IIa clinical trials [24], showing that $V^{IV}O$ complexes are more potent in decreasing the glucose concentration in blood serum than the its corresponding $VOSO_4$ salt [25].

The stability of the vanadium complexes in +IV oxidation state is interconnected with possible active form in the organism for potential anti-diabetic compounds; in fact, *in vivo* EPR studies monitoring blood circulation in rats suggested that, when vanadium is administered as $VOSO_4$, at least 90% is present in oxidation state +IV in nearly all organs studies [26]. Furthermore, the absorption in the gastrointestinal tract, its transport in the blood and uptake by the target cells has a synergistic effect on the assimilation of the V complex in the human body [27]. Also, another fact which influences the interaction with the blood and intracellular protein is the geometry of the vanadium complex in the aqueous solution at

physiological pH and its thermodynamic stability [28]. Consequently, a thorough knowledge of the vanadium complexes, the thermodynamic stability of the formed species, and their interaction with proteins are of fundamental importance in understanding mechanism of action of pharmacologically active V compounds [29-31].

Additionally ligands containing hydrazones (−NH−N = CRR′) and azines (RR′C = NN = CRR′), {R and R′ = H, alkyl, aryl}, are known to exhibit a wide range application in the field of analytical [32] and medicinal chemistry [33]. Hydrazone moieties act as an important pharmacophoric cores of several anti-cancer, anti-inflammatory, anti-nociceptive and anti-platelet drugs [34]. Hydrazones in combination with heterocycles display a wide range of biological activity [35–37] and also enhances the pharmacological activity [38]. Again, the derivatives of heterocyclic compound, quinoline are well-known for their several biological application [39,40]. Anticancer drugs containing quinoline derivatives are able to control the neoplasmic progression by inhibiting enzymes such as protein kinases, telomerase, topoisomerases, histone acetyltransferases, protein phosphatase Cdc25 and deacetylases [41]. This area is of current interest and is quite evident from the large number of biologically active natural products and pharmaceuticals appended with a quinoline moiety or heterocyclic backbone as a structural framework [42]. In view of the importance of these compounds, currently significant amount of attention is being paid to synthesize several derivatives of the heterocyclic moieties. As quinoline moiety itself has very limited applications but quinoline scaffold containing various others biologically active moieties have been selectively used to develop a wide range molecule with medicinal benefits [42].

Keeping these observations in mind and in continuation of our research, in this paper we have reported the synthesis of eight hexa-coordinated mononuclear mixed-ligand oxidovanadium(IV) complexes [VO($\mathbf{L}^{x}$)($\mathbf{L}^{\text{N-N}}$)] (**1-8**) of aroylhydrazone ligands incorporating quinolone moiety. The systems $V^{IV}O^{2+}$/$\mathbf{L}^{x}$, $V^{IV}O^{2+}$/$\mathbf{L}^{x}$/bipy and $V^{IV}O^{2+}$/$\mathbf{L}^{x}$/phen have been

studied in solution, and particularly around the physiological pH, with a view to evaluate the behavior of these species in the biological media. The coordination mode of the ligands to the $V^{IV}O^{2+}$ ion has also been evaluated. Finally, the interaction of the $V^{IV}O$ species with model proteins, like lysozyme (Lyz) and cytochrome *c* (Cyt), and bovine serum albumin (BSA) was evaluated and the complexes have been probed for their DNA binding ability. The interaction studies with Lyz and Cyt were carried out through the combined application of instrumental Electron Paramagnetic Resonance (EPR), and ElectroSpray Ionization Mass Spectroscopy, (ESI-MS), computational methods (Density Functional Theory, DFT), and the interaction with bovine serum albumin (BSA) was analyzed through fluorescence spectroscopy, while the interaction with Calf Thymus DNA (CT-DNA) was studied through UV-vis absorption titration and fluorescence spectral studies. The results could provide a comprehensive understanding of the behaviour of vanadium–quinoline complexes with the aim of the possible experimentation as potential metal based drugs.

2. Experimental Section

2.1 General Methods and Materials

All chemicals were purchased from commercial sources and used without further purification. $[VO(acac)_2]$ was prepared as described in the literature [43]. Reagent grade solvents were dried and distilled prior to use. Oxidovanadium(IV) sulfate trihydrate ($VOSO_4 \cdot 3H_2O$), 2,2'-bipyridine (bipy), 1,10-phenanthroline (phen), 1-methylimidazole (MeIm), DMSO and DMF were purchased from Sigma-Aldrich and Lancaster and were used without further purification. Lysozyme from chicken egg white (abbreviated with Lyz; product number 62970), cytochrome *c* from equine heart (abbreviated with Cyt; product number C2506) were Sigma-Aldrich products and were used without further purification, bovine serum albumin (BSA) and calf-thymus DNA were procured from Sigma Aldrich

(USA) and SRL (India) (biochemistry grade) respectively. Ultrapure water was obtained through the purification system Millipore MilliQ Academic. Elemental analysis were performed on a Vario ELcube CHNS Elemental analyzer. Melting points were measured using melting point apparatus (Model No. MR1740124). IR spectra were recorded on a Perkin-Elmer Spectrum RXI spectrophotometer. ^{1}H and ^{13}C NMR spectra were recorded on a Bruker Ultrashield 400 MHz spectrometer in presence of $SiMe_4$ as an internal standard. Electronic spectra were recorded on a Lamda25, PerkinElmer spectrophotometer. ElectroSpray Ionization mass spectra (ESI-MS) were obtained with a SQ-300 MS instrument (section 3.5) or with a Thermo Fisher Scientific Q Exactive™ Plus Hybrid Quadrupole-Orbitrap™ (section 3.13). ESI-MS spectra were analysed by using Thermo Xcalibur 3.0.63 software (Thermo Fisher Scientific) and the average deconvoluted monoisotopic masses were obtained through the Xtract tool integrated in the software. Electrochemical data were collected using CH-Instruments (Model No. CHI6003E) using DMSO as a solvent and TBAP (tetra butyl ammonium perchlorate) as the supporting electrolyte at 298 K in a dry nitrogen atmosphere using a Pt working electrode, Pt auxiliary electrode, and an Ag/AgCl as reference electrode. EPR spectra were recorded at 120 K with an X-band (ca. 9.4 GHz) Bruker EMX spectrometer equipped with an HP 53150A microwave frequency counter.

2.2 Synthesis of Ligands ($\mathbf{H_2L^x}$) (x = 1–4)

The 2-hydroxy-3-quinolinecarboxaldehyde were prepared from 2-chloro-3-quinolinecarboxaldehyde by a known method, reported earlier [44]. Whereas the aroylhydrazone ligands, $\mathbf{H_2L^x}$ were prepared by the condensation of the previously synthesized 2-hydroxy-3-quinolinecarboxaldehyde and the respective acid hydrazide (2-furoic hydrazide = $\mathbf{H_2L^1}$, 2-thiophenecarboxylic acid hydrazide = $\mathbf{H_2L^2}$, 1-naphthoic hydrazide = $\mathbf{H_2L^3}$ and 3-hydroxy-2-naphthoic hydrazide = $\mathbf{H_2L^4}$) in 1:1 ratio in ethanol by

following a reported procedure [45]. The resulting yellow compounds were filtered, washed with ethanol and dried over fused $CaCl_2$ overnight. The elemental analysis, NMR (^1H and ^{13}C) and IR data, clearly confirmed their preparation. The synthesis of the ligands is illustrated in **Scheme 1**.

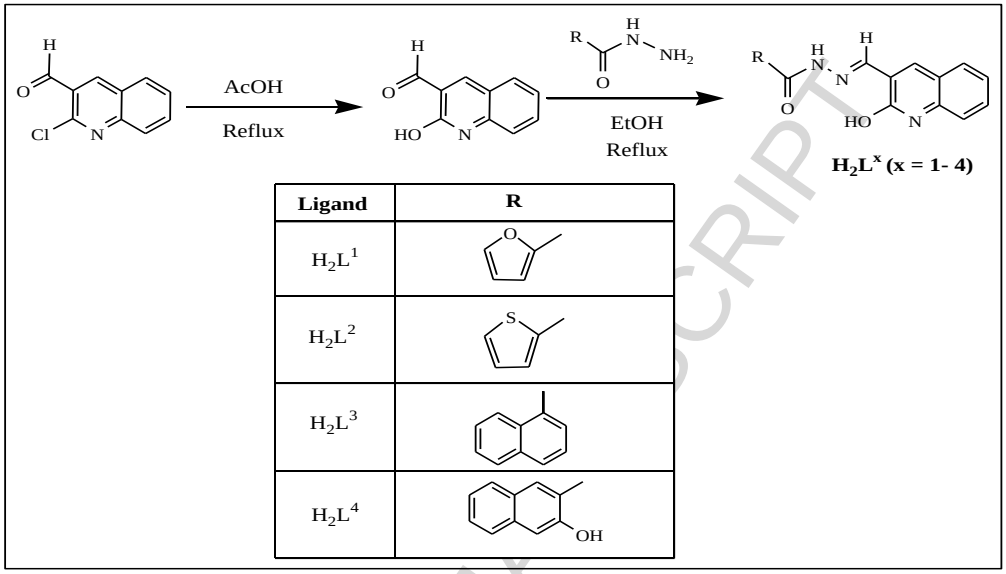

Scheme 1. Schematic diagram of the ligands (**H_2L^x**)

H_2L^1: Yield: 69%. Anal. calcd. for $C_{15}H_{11}N_3O_3$: C, 64.05; H, 3.94; N, 14.94. Found: C, 64.12; H, 3.72; N, 14.83. Mp: 156−160 °C. IR (KBr pellet, cm^{-1}): 3249 *ν*(O–H); 3056 *ν*(N–H); 1654 *ν*(C=O); 1546 *ν*(C=N). ^1H NMR (400 MHz, DMSO-d_6): *δ* 12.09 (s, 1H, quinoline–OH), 12.02 (s, 1H, NH), 8.70 (s, 1H, HC=N–), 8.47–7.19 (m, 8H, Aromatic). ^{13}C NMR (100 MHz, DMSO-d_6): *δ* 161.50 (CO–N), 158.19 (N=CH–), 152.36–113.59 (13C, aromatic).

H_2L^2: Yield: 74%. Anal. calcd. for $C_{15}H_{11}N_3O_2S$: C, 60.59; H, 3.73; N, 14.13. Found: C, 60.54; H, 3.69; N, 14.28. Mp: 134−140 °C. IR (KBr pellet, cm^{-1}): 3245 *ν*(O–H); 3052 *ν*(N–H); 1656 *ν*(C=O); 1544 *ν*(C=N). ^1H NMR (400 MHz, DMSO-d_6): *δ* 12.10 (s, 1H, quinoline–OH), 12.07 (s, 1H, NH), 8.70 (s, 1H, HC=N–), 8.44–6.69 (m, 8H, Aromatic). ^{13}C NMR (100 MHz, DMSO-d_6): *δ* 161.48 (CO–N), 154.75 (N=CH–), 146.83–112.59 (13C, aromatic).

H_2L^3: Yield: 72%. Anal. calcd. for $C_{21}H_{15}N_3O_2$: C, 73.89; H, 4.43; N, 12.31. Found: C, 73.86; H, 4.46; N, 12.07. Mp: 162−169 °C. IR (KBr pellet, cm^{-1}): 3243 *ν*(O–H); 3052 *ν*(N–H); 1660 *ν*(C=O); 1552 *ν*(C=N). ^{1}H NMR (400 MHz, DMSO-d_6): *δ* 12.08 (s, 1H, quinoline–OH), 11.26 (s, 1H, NH), 8.66 (s, 1H, HC=N–), 8.51–7.20 (m, 12H, Aromatic). ^{13}C NMR (100 MHz, DMSO-d_6): *δ* 164.48 (CO–N), 161.42 (N=CH–), 143.66–110.92 (19C, aromatic).

H_2L^4: Yield: 77%. Anal. calcd. for $C_{21}H_{15}N_3O_3$: C, 70.58; H, 4.23; N, 11.76. Found: C, 70.62; H, 4.29; N, 11.75. Mp: 175−183 °C. IR (KBr pellet, cm^{-1}): 3440 *ν*(O–H), 3211 *ν*(O–H); 3039 *ν*(N–H); 1652 *ν*(C=O); 1545 *ν*(C=N). ^{1}H NMR (400 MHz, DMSO-d_6): *δ* 12.19 (s, 1H, naphthalene –OH), 12.11 (s, 1H, quinoline–OH), 11.35 (s, 1H, NH), 8.69 (s, 1H, HC=N–), 8.52–7.20 (m, 11H, Aromatic). ^{13}C NMR (100 MHz, DMSO-d_6): *δ* 164.60 (CO–N), 161.49 (N=CH–), 146.83–112.59 (19C, aromatic).

*2.3 Synthesis of oxidovanadium(IV) [VO($\mathbf{L}^x$)($\mathbf{L}^{N-N}$)] compounds (**1**–**8**)*

In order to synthesize the eight mixed-ligand oxidovanadium(IV) complexes [VO($\mathbf{L}^x$)($\mathbf{L}^{N-N}$)] (**1**-**8**) where $\mathbf{L}^x$ = $\mathbf{L}^1$–$\mathbf{L}^4$ is four quinoline based aroylhydrazones ($\mathbf{H_2L}^x$) and $\mathbf{L}^{N-N}$ is *N*,*N*-donor bases like bipy (**1**, **3**, **5** and **7**) and phen (**2**, **4**, **6** and **8**), the metal precursor [$V^{IV}O(acac)_2$] (1.0 mmol) was added to a hot solution of the corresponding ligand $\mathbf{H_2L}^x$ (1.0 mmol) in CH_3CN (30 mL), the mixture was refluxed for 1 h under nitrogen atmosphere resulting in a brown solution, then a stoichiometric amount of 2,2'-bipyridine (**1**, **3**, **5** and **7**) or 1,10-phenanthroline (**2**, **4**, **6** and **8**) (1.0 mmol) was added and was further refluxed for ca 2 h. Brown crystals of **1** and **6** suitable for X-ray measurements were obtained from the reaction mixture which was then filtered, washed thoroughly with ethanol and dried. However, the X-ray quality crystals for the rest of the compounds (**2**, **3**, **4**, **5**, **7** and **8**) could not be isolated. The synthesis of the complexes is illustrated in **Scheme 2**.

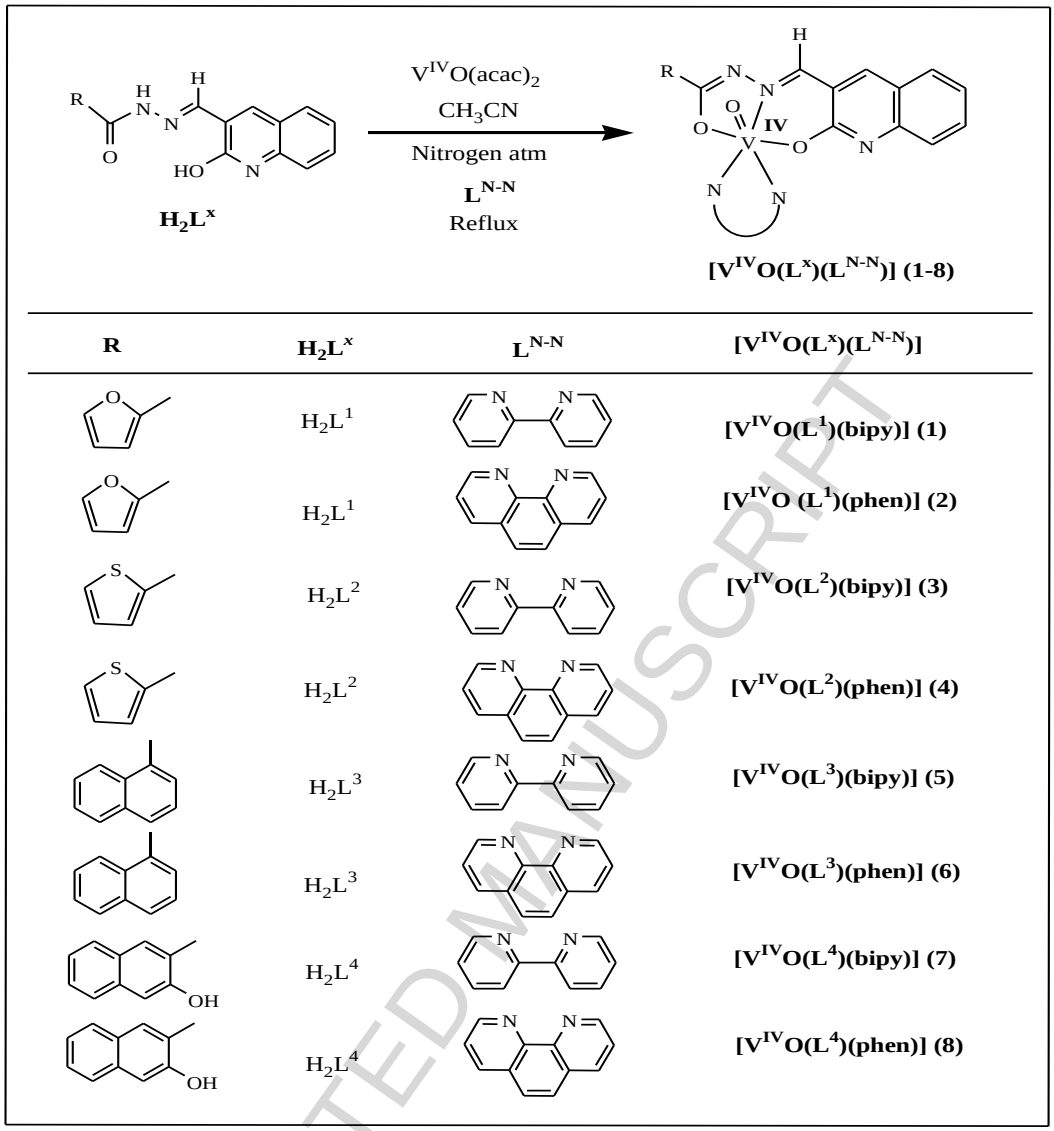

R	H_2L^x	L^{N-N}	$[V^{IV}O(L^x)(L^{N-N})]$
	H_2L^1		$[V^{IV}O(L^1)(bipy)]$ (1)
	H_2L^1		$[V^{IV}O(L^1)(phen)]$ (2)
	H_2L^2		$[V^{IV}O(L^2)(bipy)]$ (3)
	H_2L^2		$[V^{IV}O(L^2)(phen)]$ (4)
	H_2L^3		$[V^{IV}O(L^3)(bipy)]$ (5)
	H_2L^3		$[V^{IV}O(L^3)(phen)]$ (6)
	H_2L^4		$[V^{IV}O(L^4)(bipy)]$ (7)
	H_2L^4		$[V^{IV}O(L^4)(phen)]$ (8)

Scheme 2. Schematic representation of syntheses of oxidovanadium(IV) complexes, **$[V^{IV}O(L^x)(L^{N-N})]$** (**1–8**).

$[V^{IV}O(L^1)(bipy)]$ (1): Yield: 68%. Anal. Calcd. for $C_{25}H_{17}N_5O_4V$: C, 59.77; H, 3.41; N, 13.94. Found: C, 59.90; H, 3.44; N, 13.86. IR (KBr pellet, cm^{-1}): 1603 *ν*(C=N); 1272 *ν*(C–O); 965 *ν*(V=O); 557 *ν*(V–O); 444 *ν*(V–N); 1510, 1422 and 730 *ν*(V–bipy). UV–Vis (DMSO) [λ_{max}, nm (ε, M^{-1} cm^{-1})]: 727 (42), 401 (4907), 372 (9805), 272 (14992). ESI-MS: m/z 501.99 $[M]^+$.

[$V^{IV}O(L^1)$(phen)] (2): Yield: 68%. Anal. Calcd. for $C_{27}H_{17}N_5O_4V$: C, 61.61; H, 3.26; N, 13.30. Found C, 61.56; H, 3.29; N, 13.23. IR (KBr pellet, cm^{-1}): 1619 *ν*(C=N); 1262 *ν*(C–O); 956 *ν*(V=O); 566 *ν*(V–O); 432 *ν*(V–N); 1504, 1420 and 730 *ν*(V–phen). UV–Vis (DMSO) [λ_{max}, nm (ε, M^{-1} cm^{-1})]: 739 (24), 404 (4469), 365 (9106), 265 (15013). ESI-MS: m/z 524.19 $[(M-2H)]^+$.

[$V^{IV}O(L^2)$(bipy)] (3): Yield: 74%. Anal. Calcd. for $C_{25}H_{17}N_5O_3SV$: C, 57.92; H, 3.31; N, 13.51. Found C, 57.97; H, 3.27; N, 13.46. IR (KBr pellet, cm^{-1}): 1594 *ν*(C=N); 1268 *ν*(C–O); 957 *ν*(V=O); 560 *ν*(V–O); 444 *ν*(V–N); 1494, 1430 and 733 *ν*(V–bipy). UV–Vis (DMSO) [λ_{max}, nm (ε, M^{-1} cm^{-1})]: 732 (18), 401 (4501), 370 (9541), 266 (15221). ESI-MS: m/z 517.36 $[M-H]^+$, 541.41 $[M+Na]^+$.

[$V^{IV}O(L^2)$(phen)] (4): Yield: 74%. Anal. Calcd. for $C_{27}H_{17}N_5O_3SV$: C, 59.78; H, 3.16; N, 12.91. Found C, 59.71; H, 3.14; N, 12.95. IR (KBr pellet, cm^{-1}): 1603 *ν*(C=N); 1271 *ν*(C–O); 960 *ν*(V=O); 568 *ν*(V–O); 440 *ν*(V–N); 1498, 1426 and 732 *ν*(V–phen). UV–Vis (DMSO) [λ_{max}, nm (ε, M^{-1} cm^{-1})]: 748 (21), 402 (4454), 368 (9246), 271 (15562). ESI-MS: m/z 541.14 $[M-H]^+$.

[$V^{IV}O(L^3)$(bipy)] (5): Yield: 68%. Anal. Calcd. for $C_{31}H_{21}N_5O_3V$: C, 66.20; H, 3.76; N, 12.45. Found: C, 66.26; H, 3.71; N, 12.40. IR (KBr pellet, cm^{-1}): 1619 *ν*(C=N); 1270 *ν*(C–O); 964 *ν*(V=O); 575 *ν*(V–O); 433 *ν*(V–N); 1498, 1436 and 736 *ν*(V–bipy). UV–Vis (DMSO) [λ_{max}, nm (ε, M^{-1} cm^{-1})]: 734 (27), 403 (4492), 372 (9351), 266 (15662). ESI-MS: m/z 561.60 $[M]^+$.

[$V^{IV}O(L^3)$(phen)] (6): Yield: 69%. Anal. Calcd. for $C_{33}H_{21}N_5O_3V$: C, 67.58; H, 3.61; N, 11.94. Found C, 67.55; H, 3.66; N, 11.95. IR (KBr pellet, cm^{-1}): 1603 *ν*(C=N); 1267 *ν*(C–O); 957 *ν*(V=O); 572 *ν*(V–O); 438 *ν*(V–N); 1504, 1424 and 730 *ν*(V–phen). UV–Vis (DMSO) [λ_{max}, nm (ε, M^{-1} cm^{-1})]: 736(15), 406 (4406), 372 (9225), 264 (15493). ESI-MS: m/z 587.54 $[M+H]^+$.

[$V^{IV}O(L^4)$(bipy)] (7): Yield: 68%. Anal. Calcd. for $C_{31}H_{21}N_5O_4V$: C, 64.36; H, 3.66; N, 12.11. Found: C, 64.39; H, 3.59; N, 12.07. IR (KBr pellet, cm^{-1}): 3419 *v*(O–H); 1610 *v*(C=N); 1275 *v*(C–O); 964 *v*(V=O); 566 *v*(V–O); 435 *v*(V–N); 1510, 1436 and 736 *v*(V–bipy). UV–Vis (DMSO) [λ_{max}, nm (ε, M^{-1} cm^{-1})]: 797 (32), 403 (4553), 360 (9321), 270 (15772). ESI-MS: m/z 577.34 $[M-H]^+$.

[$V^{IV}O(L^4)$(phen)] (8): Yield: 68%. Anal. Calcd. for $C_{33}H_{21}N_5O_4V$: C, 65.79; H, 3.51; N, 11.62. Found: C, 65.77; H, 3.57; N, 11.53. IR (KBr pellet, cm^{-1}): 3442 *v*(O–H); 1594 *v*(C=N); 1272 *v*(C–O); 978 *v*(V=O); 569 *v*(V–O); 431 *v*(V–N); 1509,1432 and 733 *v*(V–phen). UV–Vis (DMSO) [λ_{max}, nm (ε, M^{-1} cm^{-1})]: 747 (19), 406 (4603), 364 (9457), 272 (15016). ESI-MS: m/z 600.65 $[M-H]^+$.

2.4 X-ray Crystallography

Intensity data of **1** (color: black; size: 0.07 × 0.02 × 0.01 mm^3; prism) and **6** (color: dark red; size: 0.235 × 0.122 × 0.05 mm^3; prism) were collected at -183 ^oC, **1**, and -173 °C, **6** on a Bruker Kappa APEX II CCD-based 4-circle X-ray diffractometer using graphite monochromated Mo K_α radiation (λ = 0.71073 Å) of a fine focus molybdenum-target X-ray tube operating at 50 kV and 30 m. Crystal-to-detector distance was 40 mm and exposure time was 60 seconds per frame for all sets of **1** and 15 seconds for all sets of **6** with scan width of 1^o, **1**, and 0.5°, **6**. Data were integrated and scaled using the programs SAINT and SADABS (semi-empirical absorption correction from equivalents) within the APEX2 software package by Bruker [46]. R_{int} = 0.1186, **1**, and 0.0856, **6**, indicated that the data were appropriate, but coming from small samples. Structures were solved by direct methods (SHELXS, SIR97 [47]) and completed by difference Fourier synthesis with SHELXL97 [48,49]. Structure refinements were carried out on F^2 using full-matrix least-squares procedures [50], applying anisotropic thermal displacement parameters for all non-hydrogen atoms and scattering

factors from Waasmair and Kirfel [51a], and Wilson [51b], respectively. Hydrogen atoms were placed in geometrically idealized positions and constrained to ride on their parent atoms with C–H distances of 0.95Å and fixed isotropic thermal displacement parameters calculated to be $1.2U_{eq}$ of their parent atom. The furan ring of **1** is disordered at 0.63(1): 0.37(1) by 180° rotation around the C1-C41 bond. Molecular structure diagrams, showing the atom labelling schemes, were drawn with 50% displacement ellipsoids using DIAMOND [52]. CCDC 1856634, **1**, and 1856633, **6**, contain supplementary crystallographic data. These data can be obtained free of charge via http://www.ccdc.cam.ac.uk/conts/retrieving.html, or from the Cambridge Crystallographic Data Centre, 12 Union Road, Cambridge CB2 1EZ, UK; fax: +44 1223 336 033; or e-mail: deposit@ccdc.cam.ac.uk.

2.5 EPR measurements

EPR spectra were recorded at 120 K with an X-band (9.4 GHz) Bruker EMX spectrometer equipped with an HP 53150A microwave frequency counter. Anisotropic spectra were recorded dissolving the polycrystalline powder in a mixture DMF/DMSO 85/15 (v/v). Anisotropic spectra of the systems $V^{IV}O^{2+}$/$\mathbf{L}^{x}$/bipy and $V^{IV}O^{2+}$/$\mathbf{L}^{x}$/phen were measured dissolving in a mixture H_2O/DMSO 50/50 (v/v) the metal salt $VOSO_4 \cdot 3H_2O$, the ligand $\mathbf{L}^{x}$ and the co-ligand bipy or phen. The final concentration of $V^{IV}O^{2+}$ was 1.0×10^{-3} M.

The experimental values of the ^{51}V hyperfine coupling constant along the *z* axis (A_z) were determined with the software WinEPR SimFonia [53], the estimated error in A_z being $\pm 0.3 \times 10^{-4}$ cm^{-1}. The characterization of $V^{IV}O$ species in solution was based on the comparison between experimental and DFT calculated values of the ^{51}V hyperfine coupling constant along the *z* axis (A_z). With ligands provided with N or O donors, DFT methods allow calculating A_z (A_z^{calcd}) with a mean absolute percent deviation (MADP) below 3% from the experimental value [54]. For some complexes, the experimental A_z (A_z^{exptl}) were also

compared with the values estimated with the 'additivity relationship' (A_z^{estmtd}), which relates A_z to the number and type of the equatorial ligands, assigning them a specific contribution. This empirical relationship has been proved and accepted in a large number of papers [55]. The contributions of the keto-O (43.5×10^{-4} cm^{-1}), imine-N (41.6×10^{-4} cm^{-1}), phenolato-O$^-$ (38.9×10^{-4} cm^{-1}), alcoholato-O$^-$ (35.3×10^{-4} cm^{-1}), aromatic-N (40.7×10^{-4} cm^{-1}) and H_2O (45.6×10^{-4} cm^{-1}) were taken from refs [55b-c].

2.6 Preparation of the solutions for ESI-MS measurements on the systems with lysozyme and cytochrome c

The solutions were prepared by dissolving in DMSO a weighted amount of the vanadium complex (**1** or **2**) to obtain a metal ion concentration of 1.0×10^{-3} M. The complex solutions were diluted in ultrapure water (LC-MS grade, Sigma-Aldrich) and mixed with aliquots of a stock protein solution (500 μM) in order to have a metal-to-protein molar ratio of 3/1, 5/1 and 10/1 with a final protein concentration of 5 or 50 μM. The pH was not modified and in all the systems was in the range 5-6. Argon was bubbled through the solutions to ensure the absence of oxygen and avoid the oxidation of $V^{IV}O^{2+}$ ion. After the preparation of the solutions, ESI-MS spectra were recorded immediately.

2.7 DFT Calculations

All the theoretical calculations were performed with DFT methods through the software Gaussian 09 (revision C.01) [56]. The relative stability in solution of the four possible tautomers of the free ligand $\mathbf{L^1}$ in its neutral form ($\mathbf{H_2L^1}$) was calculated using the double hybrid GGA B3LYP functional combined with the Grimme's D3 correction [57] for dispersion and the 6-311++g(d,p) basis set. Geometry optimization and harmonic frequencies

were computed adopting the SMD continuum model [58], which gives good results in the prediction of solvation Gibbs energy.

The geometry and harmonic frequencies of the $V^{IV}O$ complexes were computed using the B3P86 in combination with the 6-311g basis-set according to the previous published procedure [59]. This level of theory ensures a good accuracy in the geometry optimization of V species [59d].

On the optimized structures, the ^{51}V hyperfine coupling (HFC) $\boldsymbol{A}$ tensor was simulated using the half-and-half hybrid functional BHandHLYP and the basis set 6-311+g(d), according to the previously validated method [54,60]. At a first approximation, HFC tensor $\boldsymbol{A}$ has two contributions: the isotropic Fermi contact (A^{FC}) and the anisotropic or dipolar hyperfine interaction ($\boldsymbol{A}^{D}$) [61]: $\boldsymbol{A} = A^{FC}\mathbf{1} + \boldsymbol{A}^{D}$, where $\mathbf{1}$ is the unit tensor. The values of the ^{51}V anisotropic hyperfine coupling constants along the *x*, *y* and *z* axes are $A_x = A^{FC} + A_x^D$, $A_y = A^{FC} + A_y^D$ and $A_z = A^{FC} + A_z^D$. The theory background was described in detail [54, 62]. For the $V^{IV}O^{2+}$ species the value of the hyperfine coupling constant (A_z) is generally negative, but often in literature it is reported its absolute value and this formalism is used in some points of the text.

The relative stability of the square pyramidal [VO($\mathbf{L^1}$)(H_2O)] and octahedral mixed species [VO($\mathbf{L^1}$)(bipy)] and [VO($\mathbf{L^1}$)(phen)] was calculated at the B3P86/6-311g level of theory with SMD continuum model for water [58].

2.8 Fluorescence quenching studies of Bovine Serum Albumin

Tryptophan fluorescence quenching experiment was performed to study the interaction of the complexes with proteins using Bovine Serum Albumin (BSA) in Tris–HCl buffer (pH 8) with excitation at 295 nm and emission at 340 nm, using a Fluoromax-4P spectrofluorometer (Horiba Jobin Mayer, USA). The stock solution of the BSA was prepared in Tris–HCl buffer

while those of the complexes were prepared in a mixture of DMSO/Tris–HCl buffer and were further diluted suitably in the Tris–HCl buffer to get the required concentrations. For the experiment, the quenching of the emission intensity of tryptophan residue of BSA (2 mL, 10 μM) was monitored with increasing complex concentration (0–100 μM) as quenchers.

2.9 DNA binding experiments

Absorption spectral studies

The binding propensity of the mixed-ligand oxidovanadium(IV) complexes towards DNA binding experiments was carried out through a previously described method [45] and in 50 mM Tris–HCl buffer (pH 8.0) with Shimadzu spectrophotometer (UV–2450). These experiments were performed by titration of a fixed concentration of metal complex (25 μM) against a variable CT–DNA concentration ranging from 0 to 150 μM. Also, similar experiments were performed to check the binding of the ligands to CT–DNA.

2.10 Competitive DNA binding by Ethidium bromide (EB) displacement experiment

Ethidium bromide (EB) is a DNA binding probe which binds with DNA through intercalative mode. Therefore, the competitive binding of the complexes by intercalation to CT-DNA was probed by measuring the fluorescence of EB bound CT-DNA with increasing concentration of the complexes. The experiments were performed at fluorescence intensities of EB at 605 μm (excitation 520 μm) with an increasing amount of the complex concentration (0–100 μM) by using Fluoromax 4P spectrofuorimeter (Horiba Jobin Mayer, USA).

3. Results and discussion

3.1 Synthesis

Four quinoline based aroylhydrazones ($\mathbf{H_2L^x}$) were used as ligands and 2,2′-bipyridine (bipy) or 1,10-phenanthroline (phen) as co-ligands in the present study. The reaction of $[V^{IV}O(acac)_2]$ with their corresponding ligands ($\mathbf{H_2L^x}$) and co-ligands under inert atmosphere lead to the formation of hexacoordinated mononuclear mixed-ligand oxidovanadium(IV) $[VO(\mathbf{L^x})(\mathbf{L^{N\text{-}N}})]$ complexes (**1**–**8**). The synthesis of the complexes is illustrated in **Scheme 2**. The reactions produced large quantities of pure crystalline products with good yield (~75%). However, suitable single crystals for X-ray measurements could only be obtained for the complexes **1** and **6**. The complexes are moderately soluble in CH_2Cl_2, DMF and DMSO and sparingly soluble in EtOH, MeOH and CH_3CN. Further, the solid state stability of all complexes has also been investigated through time dependent IR and UV-vis spectroscopy in open air at 28°C. The representative spectrum of complex 4 and 5 has been depicted in Figure **S1** (IR) and **S2** (UV-vis).

3.2 Spectral Characteristics

IR data of the ligands, $\mathbf{H_2L^{1\text{–}4}}$ and their corresponding metal complexes (**1–8)** are given in the experimental section. All the ligands exhibit a band in the region of 3249–3211 cm^{-1} assignable to the aromatic –OH stretching vibration of the quinoline moiety, which is absent in the corresponding metal complexes due to its coordination. However, the presence of a band in the region 3442–3419 cm^{-1} in case of complexes **7** and **8** can be assigned to the uncoordinated –OH group attached to the naphthalene moiety of ligand $\mathbf{H_2L^4}$. Also, the bands for –NH and –C=O stretching vibration of the ligands appear at 3039–3056 cm^{-1} and 1652–1660 cm^{-1} region respectively and are absent in spectra of their corresponding complexes. All complexes also exhibit three new bands in the region 1262–1275 cm^{-1}, 566–575 cm^{-1} and

431–444 cm^{-1} are attributed to C–O, V–O and V–N stretching vibration respectively [63a]. The bands observed in the window 1494–1510 cm^{-1}, 1422–1436 cm^{-1} and 730–736 cm^{-1} are characteristic for 2,2′-bipyridine or 1,10-phenantroline ligand, which also observed in the other d-electron metal complexes with phen/bipy as a ligand [63b]. There is an appearance of additional new strong bands in the range 978–956 cm^{-1} due to ν(V=O) stretching (**1**–**8**), which are in agreement with the V=O groups present in the oxidovanadium complexes [45,59h,63c].

The electronic spectra of all the complexes were recorded in DMSO and are very similar in nature. The spectral data of the complexes are given in the Experimental section and the representative spectrum of **6** is shown in **Figure 1**. There are three strong absorptions bands observed in the wavelength range from 401–264 nm. The lower energy absorption bands in this range may be assigned as ligand to metal charge transfer (LMCT) transitions [64,65] while the higher energy absorptions as ligand centered transitions [66,67]. Low intensity peaks observed in the higher wavelength range of 797−727 nm, are due to the low energy forbidden d-d transition of the respective complexes [68].

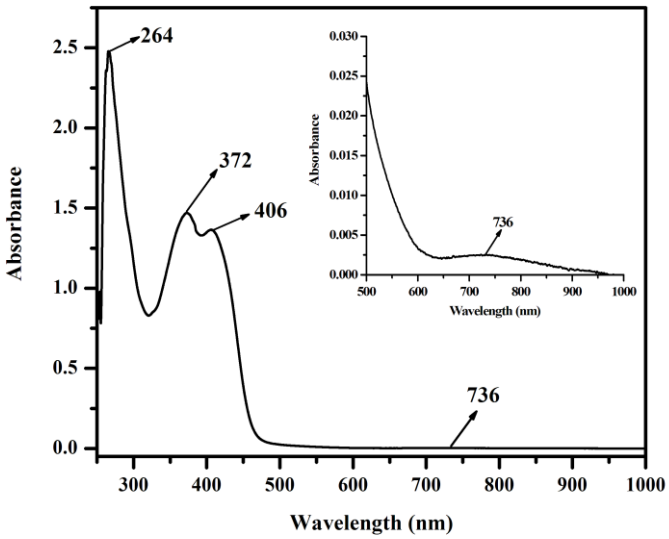

Figure 1. UV–vis spectrum of [$V^{IV}O$(**L^3**)(phen)] (**6**) (1.6×10^{-4} M) in DMSO.

^{1}H and ^{13}C NMR of the ligands (**H_2L^x**) were recorded in DMSO-d_6. The ^{1}H spectra of the free ligands exhibit resonance in the range δ 12.18–12.08 ppm due to the quinoline –OH proton, δ 12.07–11.26 ppm due to –NH proton and δ 8.70–8.66 ppm due to (–HC=N) proton respectively. Whereas all the aromatic protons of the ligands are clearly observed as multiplets in the expected region, δ 8.52–6.69 ppm [68-70].

From the ^{13}C NMR spectra, it is found that, signals for (CO–N) and (N=CH–) carbon resonates in the range, δ 164.60–161.48 ppm and 161.49–154.75 ppm respectively. Furthermore appearance of signals in the range δ 152.36–110.92 ppm due to aromatic carbon confirms the formation of the ligands [71].

ESI-MS of the complexes, **1**–**8** (Figures **S3-S10)** were recorded in DMSO employing complex concentration of 100 pmol/μL. The characteristic molecular ion peaks for complexes (**1**–**8**) appear at m/z 501.99 $[M]^+$(**1**), 524.19 $[M\text{-}2H]^+$(**2**), 517.36 $[M\text{-}H]^+$(**3**), 541.14 $[M\text{-}H]^+$(**4**), 561.60 $[M]^+$(**5**), 587.54 $[M+H]^+$(**6**), 577.34 $[M\text{-}H]^+$(**7**) and 600.65 $[M\text{-}H]^+$(**8**) respectively. In addition to the molecular ion peak, complex **3** shows one additional peak at m/z 541.41, attributed to $[M+Na]^+$.

3.3 Electrochemical Properties

The redox activity of complexes **1**–**8** was studied in DMSO solution in presence of 0.1 M TBAP as an electrolyte with cyclic voltammetry, using a Pt working and an auxiliary electrode, and Ag/AgCl as reference electrode. The voltammogram of all the complexes shows similar type of pattern and the redox potential data of all the complexes are summarized in **Table 1** and **Table S1**. As a representative, the voltammogram of $[V^{IV}O(\mathbf{L^1})(phen)]$ (**2**) shown in **Figure 2**, has been discussed herein. It is observed that in the cathodic region, there is a V(IV) to V(III) reduction, which corresponds to a quasi-reversible

single electron transfer of $E_{1/2}$ value at −1.28 V [66]. On the other hand, in the anodic region an irreversible single electron response at 0.42 V was observed which may be assignable to the V(IV)/V(V) oxidation [72]. Whereas, the irreversible anodic response at 0.97 V and cathodic response observed at –1.10 V and –1.78 V may be attributed to the ligand centered oxidation and reduction respectively [72]. The representative voltammogram of the ligand $\mathbf{H_2L^{1-2}}$ are shown in **Figure S11**. The single electron processes were also verified by maintaining the identical experimental conditions and by comparing its current height with that of the standard ferrocene−ferrocenium couple. The quasi-reversible nature of the redox processes was confirmed by comparing the voltammogram at different scan rates.

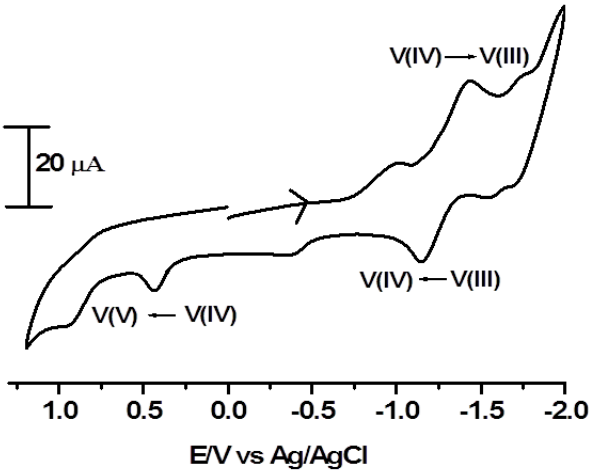

Figure 2. Cyclic voltammogram of [$V^{IV}O$(**L**^{1})(phen)] (**2**) in DMSO with 0.1M TBAP at a scan rate of 50 mV s^{-1} in presence of dry nitrogen atmosphere at 298 K.

Table 1. Cyclic voltammetric behavior of the $V^{IV}O$ complexes at 298 K in DMSO.[a]

Complex	E^{a}_{P} (V)	$E^{c}_{1/2}$ (V)	ΔE^{c}_{P} (mV)
1	0.44	-1.54	141
2	0.42	-1.28	280

3	0.46	-1.52	130
4	0.48	-1.26	265
5	0.41	-1.55	162
6	0.45	-1.31	292
7	0.43	-1.53	135
8	0.47	-1.27	270

[a] In DMSO at a scan rate of 50 mV s^{-1}. $E_{1/2} = (E_{pa} + E_{pc})/2$, where E_{pa} and E_{pc} are anodic and cathodic peak potentials vs. Ag/AgCl, respectively. $\Delta E^{c}_{P} = E_{pa} - E_{pc}$.

*3.4 Description of X-ray structure of **1** and **6***

The solid state structures of the complexes **1** and **6** were characterized by single-crystal X-ray diffraction technique. Complex **1** crystallizes triclinic, space group $P\bar{1}$, complex **6** monoclinic, space group $P2_1/n$. Crystal data and refinement details are given in **Table 2**. An overview on the solid state conformation of both complexes is shown in **Figure 3**. Selected bond distances and angles are given in **Table 3**. The structure of the complexes contains a discrete unit of monomeric vanadium(IV) species with a VO^{2+} moiety where the central vanadium atom is coordinated with tridentate binegative ONO-donor Schiff base ligand and a neutral *N*,*N*-donor base like 2,2′-bipyridine (bipy) (for complex **1**) and 1,10-phenanthroline (phen) (for complex **2**). The Schiff base coordinated to the central vanadium metal via the quinolinol oxygen O(2), imine nitrogen N(2) and hydrazide oxygen O(1) atom, while the remaining two coordination sites are satisfied by the two nitrogen atom N(4) and N(5) of the respective *N*,*N*-donor bases. In summary, the vanadium atoms comprise distorted octahedral

$V^{IV}N_3O_3$ coordination geometries. The Schiff bases display a meridional binding mode where the *N,N*-donor bases binds at the "axial-equatorial" positions. The V–N bonds of the *N,N*-donor bases *trans* to the V=O groups [mean bond length: 1.601(2) Å] are longer [2.266(3) Å, **1;** 2.338(3) Å, **6**] compared to the other V–N bond [2.146(3) Å, **1;** 2.129(3) Å, **6**,] due to the ''*trans* effect'' from the oxido ligand. V-N bonds to the Schiff base are the shortest one [2.048(3) Å, **1**; 2.054(2) Å, **6**] of all V-N bonds. V–O(1) bonds involving the Schiff bases are 1.966(3) Å (**1**) and 1.952(2) Å (**6**), while V–O(2) bonds are 2.013(2) Å (**1**) and 2.002(2) Å (**6**), respectively.

However, the distortion observed in octahedral V centers results not only from different bond lengths but also from bond angles. Thus, as bond angles between *trans* ligands strongly deviate from linearity [∠(O2-V1-O1) = 154.7(1)°, 1, 154.8(1)°, 6; ∠(N2-V1-N5) = 164.2(1)°, 1, 160.0(1)°, 6; ∠(O3-V1-N4) = 162.4(1)°, 1, 165.1(1)°, 6] also does the bond angles between *cis* ligand from 90° (Table. 3). However, importantly there are some significant bond angle differences between **1** and **6**, indicating the high flexibility within this kind of vanadium coordination mostly expressed for ∠(O2-V1-N5) = 94.0(1)°, **1**, but 100.5(1)°, **6**, and ∠(O1-V1-N5) = 96.7(1)°, **1**, but 90.2(1)°, **6**. Via these bond angle distortions, the complexes react on the different spatial demands required by the diverse ligand environment (Figures **S12**, and **S13**) and the arrangement of the complexes in the solid state in shown in Figures **S14**, and **S15**. In the absence of hydrogen donor groups, and despite the various π-systems of the ligands, intermolecular interactions seems to be restricted to van-der Waals ones. The formation of π-π-interactions seems to be suppressed in this kind of complexes as the rigid and basically flat ligands are more or less perpendicular to each other.

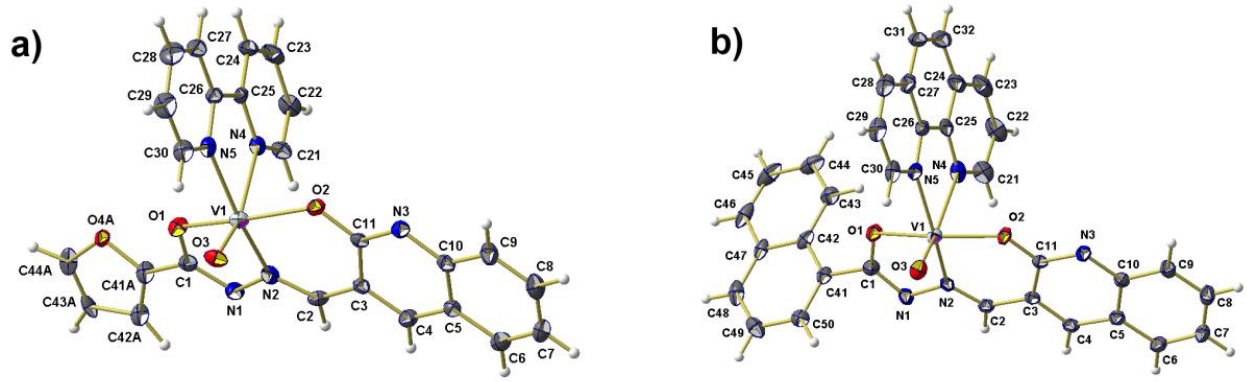

Figure 3. Ball-and-stick model of the asymmetric unit in the solid state structures of compounds (a) [$V^{IV}O(\mathbf{L}^{1})$(bipy)] (**1**) and (b) [$V^{IV}O(\mathbf{L}^{3})$(phen)] (**6**), showing the atom labeling scheme used. All non-hydrogen atoms are drawn as thermal displacement ellipsoids of the 50% level.

Table 2. Crystal data and refinement details for **1** and **6**.

Compound	**1**	**6**
Empirical formula	$C_{25}H_{17}N_5O_4V$	$C_{33}H_{21}N_5O_3V$
Mass	502.38	586.49
Temperature	90(2) K	100(2) K
Wavelength	0.71073 Å	
Crystal system	Triclinic	Monoclinic
Space group	$P\bar{1}$	$P2_1/n$
Unit cell dimensions	a = 8.0883(7) Å b = 10.9809(12) Å c = 12.6841(13) Å α = 73.875(7)°	a = 12.5155(5) Å b = 10.7549(5) Å c = 19.6211(9) Å α = 90°

	β = 78.433(6)° γ = 82.260(7)°	β = 93.426(2)° γ = 90°
Volume	1056.5(2) $Å^3$	2636.3(2) $Å^3$
Z	2	4
Density (calculated)	1.579 Mg/m^3	1.478 Mg/m^3
Absorption coefficient	0.516 mm^{-1}	0.423 mm^{-1}
F(000)	514	1204
Θ range for data collection	2.22 - 25.00°.	1.98 - 25.00°
Reflections collected	24742	92511
Independent reflections	3721 [R_{int} = 0.1186]	4650 [R_{int} = 0.0856]
Completeness to Θ = 25.00°	99.9 %	100.0 %
Limiting indices	-9<=h<=9, -13<=k<=13, -15<=l<=15	-14<=h<=14, -12<=k<=12, -23<=l<=23
Refinement method	Full-matrix least-squares on F^2	
Data/restraints/parameters	3721 / 22 / 323	4650 / 0 / 379
Goodness-of-fit on F^2	1.001	1.030
Final R indices [I>2σ(I)]	R1 = 0.0532 wR2 = 0.0923	R1 = 0.0515 wR2 = 0.1289
R indices [all data]	R1 = 0.1116 wR2 = 0.1110	R1 = 0.0692 wR2 = 0.1420
Largest diff. peak and hole	0.350 and -0.439 $eÅ^{-3}$	1.821 and -0.438 $eÅ^{-3}$

Table 3. Selected bond distances and angles for the vanadium coordination of **1** and **6**.

	1	**6**
Bond distances (Å)		
V(1)–O(1)	1.966(3)	1.952(2)
V(1)–O(2)	2.013(2)	2.002(2)
V(1)–O(3)	1.601(2)	1.601(2)
V(1)–N(2)	2.048(3)	2.054(2)
V(1)–N(4)	2.146(3)	2.129(2)
V(1)–N(5)	2.266(3)	2.338(3)
N(1)-N(2)	1.403(4)	1.404(3)
Bond angles (°)		
O(3)-V(1)-O(1)	100.9(1)	100.3(1)
O(3)-V(1)-O(2)	100.8(1)	101.9(1)
O(2)-V(1)-O(1)	154.7(1)	154.8(1)
O(3)-V(1)-N(2)	104.3(1)	104.2(1)
O(2)-V(1)-N(2)	87.3(1)	86.5(1)
O(1)-V(1)-N(2)	76.4(1)	76.6(1)
O(3)-V(1)-N(5)	90.8(1)	93.0(1)
O(2)-V(1)-N(5)	94.0(1)	100.5(1)
O(1)-V(1)-N(5)	96.7(1)	90.2(1)
N(2)-V(1)-N(5)	164.2(1)	160.0(1)
O(3)-V(1)-N(4)	162.4(1)	165.1(1)
O(2)-V(1)-N(4)	82.2(1)	78.5(1)

O(1)-V(1)-N(4)	79.5(1)	83.1(1)
N(2)-V(1)-N(4)	92.9(1)	90.5(1)
N(5)-V(1)-N(4)	71.7(1)	72.9(1)

3.5 Optimization of the free ligand structure

The structure of the free ligands (**H_2L^1**, **H_2L^2**, **H_2L^3** and **H_2L^4**) is shown in **Scheme 3**. Since the ligands can exist in solution in several tautomeric forms, the relative stability of the tuatomers for **H_2L^1** was calculated in water using SMD continuum model [58]. The results indicate that the most stable tautomer is that with the keto and amide groups (the structure represented on the left in **Figure S16a**), followed by the tautomer in the enolic form on O_1 and amide on O_2 (**Figure S16b**) with a difference in Gibbs energy of 8.6 kcal/mol. This is in agreement with the experimental data reported in the literature for 2-hydroxyquinoline, for which in polar solvents the keto is more stable than the enol tautomer by about 5 kcal/mol [73]. These findings are also coherent with the results on acetamide, for which the energy of the iminol is higher by 12-14 kcal mol^{-1} than that of the amide form [74]. The relative order of Gibbs energy is reported in **Table 4**. The $V^{IV}O$ complexes **1**–**8** were formed by the bianionic ligands upon deprotonation of the two amide groups, $CO_{(1)}NH$ and $CO_{(2)}NH$.

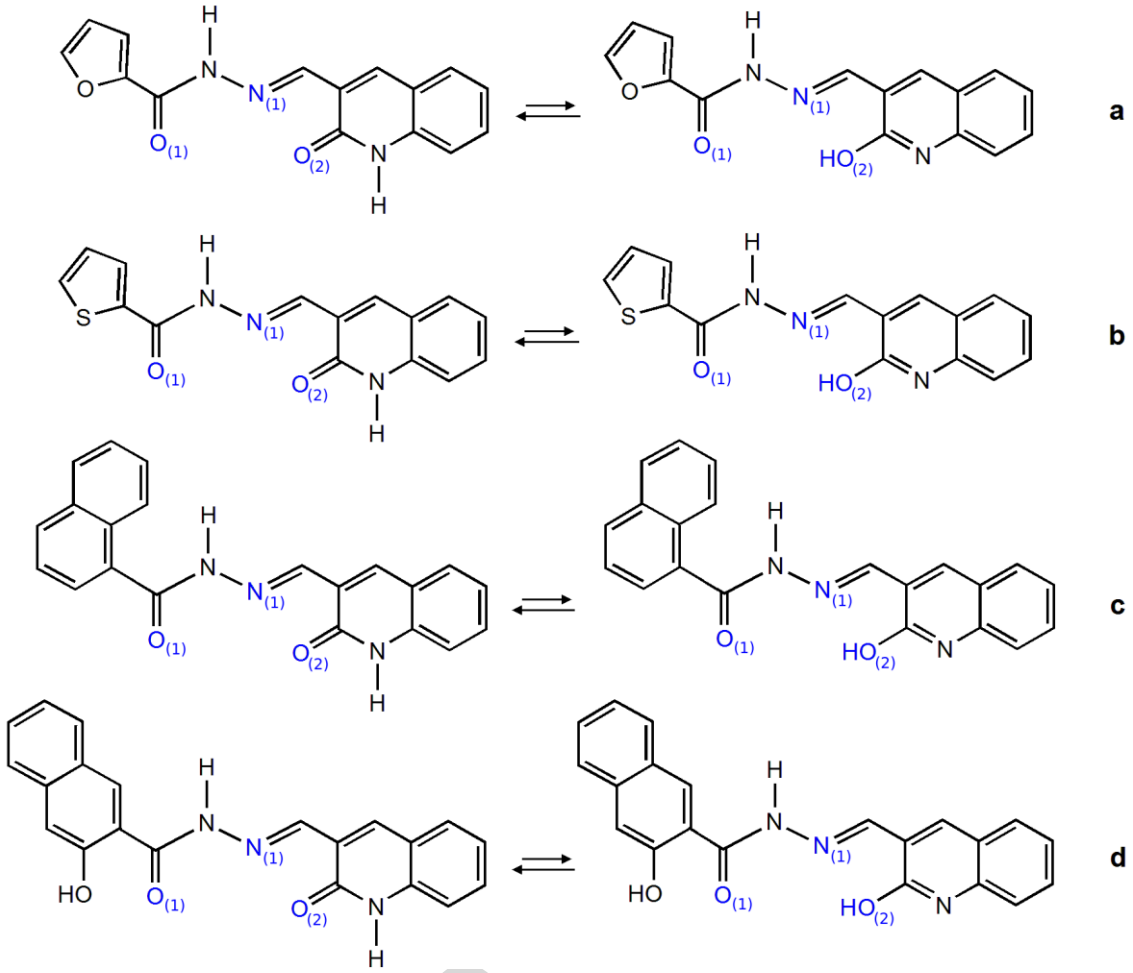

Scheme 3. Keto-amide and keto-iminol tautomers of the four ligands: a) $\mathbf{H_2L^1}$; b) $\mathbf{H_2L^2}$; c) $\mathbf{H_2L^3}$ and d) $\mathbf{H_2L^4}$.

Table 4. Gibbs energy calculated for the tautomers of $\mathbf{H_2L^1}$.[a]

Structure[b]	Tautomer	E_{aq} (a.u.)	G_{aq} (a.u.)	G_{aq} (kcal/mol)	ΔG_{aq} (kcal/mol)[c]
$CO_{(1)}$, $CO_{(2)}$	Keto-amide	-968.410042	-968.220034	-607588.78	0.00
$O_{(1)}H$, $CO_{(2)}$	Enol-amide	-968.424661	-968.233787	-607580.21	8.57
$CO_{(1)}$, $O_{(2)}H$	Keto-iminol	-968.431381	-968.239882	-607576.38	12.39
$O_{(1)}H$, $O_{(2)}H$	Enol-iminol	-968.445968	-968.253536	-607567.75	21.02

[a] Calculations carried out with SMD continuum model for water using the functional B3LYP-D3 and the basis set 6-311++g(d,p). [b] The atom indexes are those reported in **Scheme 3** and **Figure S16**. [c] Values relative to the keto-amide tautomer, set as reference.

3.6 Optimization of the structure of the $V^{IV}O$ complexes

The structure of all the $V^{IV}O$ solid complexes with composition $[V^{IV}O(\mathbf{L}^{x})(\mathbf{L}^{N-N})]$, where $\mathbf{L}^{x}$ = $\mathbf{L}^{1}$-$\mathbf{L}^{4}$ and $\mathbf{L}^{N-N}$ = bipy or phen, was optimized by DFT methods following the procedure described in the literature [59]. In **Table S2** a comparison between the principal calculated and experimental bond length and angles for the X-ray structures of $[VO(\mathbf{L}^{1})(bipy)]$ (**1**) and $[VO(\mathbf{L}^{3})(phen)]$ (**6**) is summarized, while in **Figure S17** the superimposition of the X-ray and DFT optimized structures is reported. The prediction of the vanadium environment is very good with mean absolute percent deviation (MAPD) of 0.5% (**1**) and 1.0% (**6**) for the bond lengths, and 0.6% (**1**) and 3.6% (**6**) for the angles (**Table S2**). The only disagreement concerns the position of the naphthalene ring (**Figure S17b**), free to rotate around the C1–C41 bond, and this is probably due to solid state effects not considered in the calculations.

3.7 EPR characterization of the solid compounds dissolved in solution

Anisotropic EPR spectra were recorded by dissolving the polycrystalline powder of $[V^{IV}O(\mathbf{L}^{x})(bipy)]$ (**1**, **3**, **5** and **7**) and $[V^{IV}O(\mathbf{L}^{x})(phen)]$ (**2**, **4**, **6** and **8**) in DMF/DMSO mixtures. They are shown in **Figure 4** and **Figure S18**, respectively. The values of A_z were extracted simulating the spectra with the software WinEPR SimFonia [53]; the experimental and simulated spectra for **3** and **7** are represented in **Figure S19** as an example.

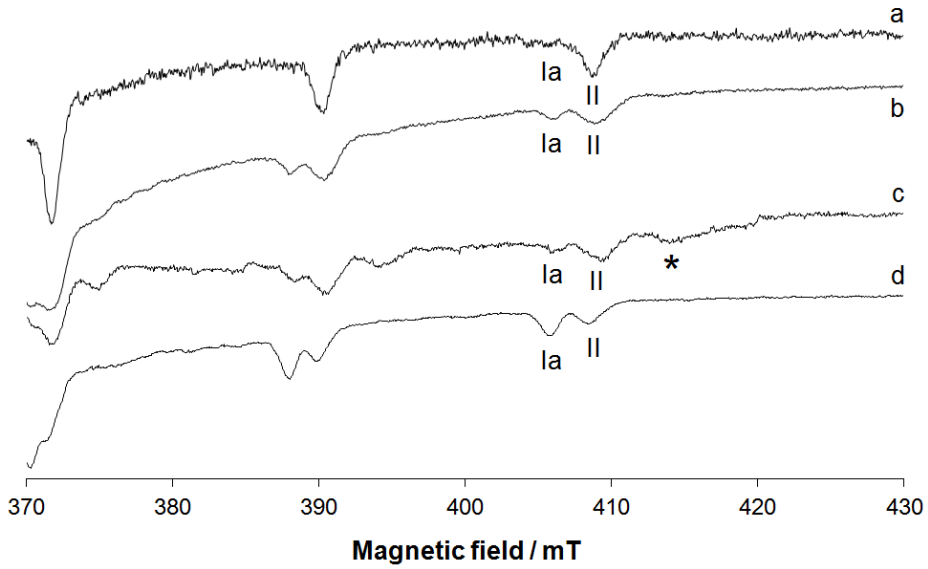

Figure 4. High field region of the X-band anisotropic EPR spectra (120 K) recorded on the solid ternary $V^{IV}O$ compounds (with bipy) dissolved in a mixture DMF/DMSO 85/15 (v/v): a) [VO(**L**^{1})(bipy)] (**1**); b) [VO(**L**^{2})(bipy)] (**3**); c) [VO(**L**^{3})(bipy)] (**5**); d) [VO(**L**^{4})(bipy)] (**7**). The M_I = 7/2 resonances of the species [VO(**L**^{x})(bipy)] (**Ia**) and [VO(**L**^{x})(Solvent)] (**II**), where Solvent stands for DMSO or DMF, are indicated. With the asterisk the M_I = 7/2 resonance of a minor species, in which the ligand **L**^{3} is presumably in a protonated form, are denoted.

The results indicate that all the systems behave similarly and that in the organic solution two species are revealed, whose resonances are indicated with **Ia** or **Ib** and **II** in **Figure 4** and **Figure S18**. The species **Ia** (with bipy) and **Ib** (with phen) are characterized by g_z = 1.950-1.951 and A_z = 159.6-160.6 × 10^{-4} cm^{-1}, whereas **II** by g_z = 1.948-1.949 and A_z = 165.6-167.4 × 10^{-4} cm^{-1}. The 'additivity relationship' suggests for the donor set observed in the solid compounds (O_1^-, N_1, O_2^-; N_{arom}^{eq}, N_{arom}^{ax}) an A_z value of 156.5 × 10^{-4} cm^{-1}; if bipy or phen are replaced by a solvent molecule a significant increase of A_z is predicted (~161-162 × 10^{-4} cm^{-1}), in agreement with what was observed.

To confirm this insight, DFT calculations were carried out to predict the ^{51}V HFC ***A*** tensor. The comparison between the calculated (A_z^{calcd}) and the experimental values (A_z^{exptl}) is summarized in **Table 5**: on the basis of these results, the two resonances **Ia** or **Ib** and **II** can be assigned to the octahedral mixed species [VO(**L**^{x})(L^{N-N})], solved by X-ray analysis, and to the square pyramidal complex [VO(**L**^{x})(Solvent)] (**II**) formed after the replacement of 2,2'-bipyridine or 1,10-phenantroline ligand by a solvent molecule (DFT simulations were performed using H_2O as representative solvent).

The relative intensity of the resonances of the two complexes (**Ia** or **Ib** and **II** in **Figure 4** and **Figure S18**) indicates that with 1,10-phenantroline the ternary species **I** is more stable than with 2,2'-bipyridine. In the systems with this latter co-ligand, instead, a larger amount of the penta-coordinated complex **II** exists.

The characterization of the species in organic solution can be confirmed analyzing the EPR spectra for the systems $V^{IV}O^{2+}$/**L**^{1}, $V^{IV}O^{2+}$/**L**^{1}/bipy and $V^{IV}O^{2+}$/**L**^{1}/phen recorded in a mixture H_2O/DMSO 50/50 (v/v) as a function of pH (see below).

Table 5. Experimental (exptl), estimated with the 'additivity relationship' (estmtd) and DFT calculated (calcd) spin Hamiltonian parameters for mixed $V^{IV}O$ complexes dissolved in DMF/DMSO 85/15 (v/v) solution.[a]

Complex	g_z^{exptl}	A_z^{exptl}	A_z^{estmtd}	A_z^{calcd}	PD [b]
[VO(**L**^{1})(bipy)] (**Ia**)	1.950 [c]	160.3 [c]	156.5	157.5	-1.7
[VO(**L**^{1})(phen)] (**Ib**)	1.951	160.2	156.5	157.1	-1.9
[VO(**L**^{1})(Solvent)] (**II**)	1.948	165.8	161-162	167.4	1.0
[VO(**L**^{2})(bipy)] (**Ia**)	1.951	160.2	156.5	157.5	-1.7
[VO(**L**^{2})(phen)] (**Ib**)	1.951	160.2	156.5	157.1	-1.9

[VO(**L**^{2})(Solvent)] (**II**)	1.949	166.6	161-162	167.1	0.3
[VO(**L**^{3})(bipy)] (**Ia**)	1.950	160.7	156.5	157.0	-2.3
[VO(**L**^{3})(phen)] (**Ib**)	1.951	160.6	156.5	156.9	-2.3
[VO(**L**^{3})(Solvent)] (**II**)	1.948	167.4	161-162	166.6	-0.5
[VO(**L**^{4})(bipy)] (**Ia**)	1.951	159.7	156.5	158.8	-0.6
[VO(**L**^{4})(phen)] (**Ib**)	1.951	159.6	156.5	157.8	-1.1
[VO(**L**^{4})(Solvent)] (**II**)	1.949	165.6	161-162	168.4	1.7

[a] A_z values reported in 10^{-4} cm^{-1}. [b] Percent deviation (PD) with respect to the absolute experimental A_z value calculated as: $100 \times [(|A_z|^{calcd} - |A_z|^{exptl})|/|A_z|^{exptl}]$. [c] Parameters measured in DMSO solution.

*3.8 Behavior of the systems $V^{IV}O^{2+}$/**L**^{x} in solution*

The systems $V^{IV}O^{2+}$/**L**^{1} and $V^{IV}O^{2+}$/**L**^{2} were studied as function of pH in a mixture H_2O/DMSO 50/50 (v/v) as representative models for the behavior of the ligands **L**^{x}. The use of DMSO is necessary for the low solubility of **L**^{x} in water; for the interpretation of the data, it must be taken into account that in this solvent mixture, due to the different dielectric constant of the two components, the experimental pH readings are larger than in water [75]. Overall, the two systems behave very similarly. At low pH values **L**^{1} and **L**^{2} act as bidentate, whereas at neutral or weak basic pH values they are tridentate upon the stepwise deprotonation of the ligands.

In **Figure 5** EPR spectra recorded in the system $V^{IV}O^{2+}$/**L**^{1} are represented as an example. The behavior of the system $V^{IV}O^{2+}$/**L**^{2} is shown in **Figure S20**. The complexation starts with the formation of $[VO(H_2\mathbf{L}^{1}\text{-}O_1,N_1)(H_2O)_2]^{2+}$ (indicated with **VI** in **Figure 5**), with the ligand in the neutral form which binds vanadium with the (O_1, N_1); H_2O; H_2O coordination mode. With increasing the pH, the ligands lose one proton forming $[VO(H\mathbf{L}^{1}\text{-}O_1^{-},N_1)(H_2O)_2]^{+}$

(indicated with **V**, (O_1^-, N_1); H_2O; H_2O coordination) and [VO(H**L**$^{\mathbf{1}}$-O_1^-,N_1,O_2)(H_2O)]$^+$ with the tridentate ligand (**IV**, (O_1^-, N_1, O_2); H_2O coordination). The values of A_z for **VI**, **V** and **IV** estimated with the 'additivity relationship' are in agreement with the experimental ones (176.3, 171.7 and 169.6 × 10^{-4} cm^{-1} estimated vs. 177.4, 175.7 and 171.0 × 10^{-4} cm^{-1} experimental).

At pH above 7, the second deprotonation of **L**$^{\mathbf{1}}$ results in the formation of [VO(**L**$^{\mathbf{1}}$)(H_2O)] (**II**), analogous to [VO(**L**$^{\mathbf{1}}$)(Solvent)] observed upon dissolution of [VO(**L**$^{\mathbf{1}}$)(**L**$^{\mathrm{N–N}}$)] in DMF/DMSO mixtures (cfr. **Figure 5** with **Figures 4** and **S18**). The values of g and A (g_z = 1.950 and A_z = 167.2 × 10^{-4} cm^{-1}) are comparable with those measured for [VO(**L**$^{\mathbf{1}}$)(Solvent)] (g_z = 1.948 and A_z = 165.8 × 10^{-4} cm^{-1}). At very basic pH values, [VO(**L**$^{\mathbf{1}}$)(H_2O)] transforms to [VO(**L**$^{\mathbf{1}}$)(OH)]$^-$ (**III**) for the deprotonation of the water ligand in the equatorial plane to give a OH^- ion; this latter species cannot be confused with the hydroxido complex $[VO(OH)_3]^-$, whose spectrum added in **Figure 5** is very different.

The structure and coordination mode of all the $V^{IV}O$ species is confirmed through the calculations of A_z at the DFT level and comparison with the experimental values. In **Table 6** the experimental (A_z^{exptl}) and DFT calculated (A_z^{calcd}) values are reported. All the optimized structures are shown in **Figure S21**, whereas the components of the ^{51}V HFC ***A*** tensor in **Table S3**.

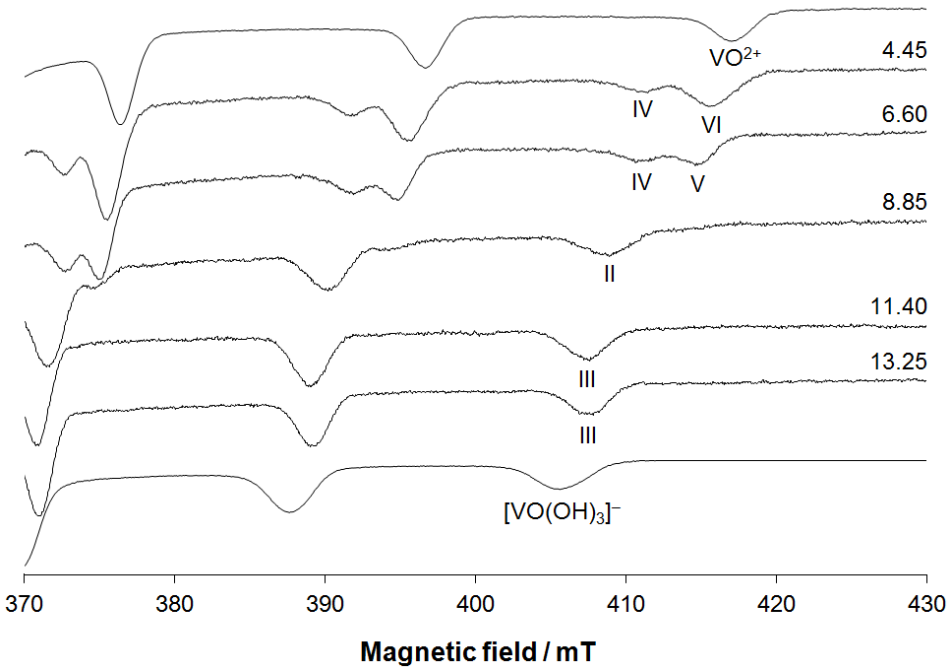

Figure 5. High field region of the X-band anisotropic EPR spectra (120 K) recorded in a mixture H_2O/DMSO 50/50 (v/v) as a function of pH in the system $V^{IV}O^{2+}$/**L**^{1} with a molar ratio of 1:1 and V concentration of 1.0×10^{-3} M. The M_I = 7/2 resonances of the species [VO(**L**^{1})(H_2O)] (**II**), [VO(**L**^{1})(OH)]$^{-}$ (**III**), [VO(H**L**^{1}-O_1^{-},N_1,O_2)(H_2O)]$^{+}$ (**IV**), [VO(H**L**^{1}-O_1^{-},N_1)(H_2O)$_2$] (**V**) and [VO(H_2**L**^{1}-O_1,N_1)(H_2O)$_2$]$^{2+}$ (**VI**) are indicated. The first and last spectrum are those of aquaion and hydroxido complex [VO(OH)$_3$]$^{-}$ (M_I = 7/2 resonances indicated with **VO^{2+}** and **[VO(OH)$_3$]$^{-}$**, respectively).

Table 6. Experimental (exptl) and DFT calculated (calcd) spin Hamiltonian parameters for $V^{IV}O$ complexes formed by **L**^{1} and **L**^{2} in H_2O/DMSO 50/50 (v/v) solution.[a]

Complex	g_z^{exptl}	A_z^{exptl}	A_z^{calcd}	PD [b]
[VO(H_2**L**^{1}-O_1,N_1)(H_2O)$_2$]$^{2+}$ (**VI**)	1.936	177.4	181.6	2.4
[VO(H**L**^{1}-O_1^{-},N_1)(H_2O)$_2$]$^{+}$ (**V**)	1.938	175.7	175.2	-0.3
[VO(H**L**^{1}-O_1^{-},N_1,O_2)(H_2O)]$^{+}$ (**IV**)	1.947	171.0	171.8	0.5

$[VO(\mathbf{L^1})(H_2O)]$ (**II**)	1.950	167.2	167.4	0.1
$[VO(\mathbf{L^1})(OH)]^-$ (**III**)	1.951	164.3	160.4	-2.4
$[VO(H_2\mathbf{L^2}\text{-}O_1,N_1)(H_2O)_2]^{2+}$ (**VI**)	1.936	178.0	181.6	2.0
$[VO(H\mathbf{L^2}\text{-}O_1^-,N_1)(H_2O)_2]^+$ (**V**)	1.938	174.6	175.3	0.4
$[VO(H\mathbf{L^2}\text{-}O_1^-,N_1,O_2)(H_2O)]^+$ (**IV**)	1.946	170.7	171.4	0.4
$[VO(\mathbf{L^2})(H_2O)]$ (**II**)	1.947	167.5	167.1	-0.2
$[VO(\mathbf{L^2})(OH)]^-$ (**III**)	1.950	164.4	160.4	-2.4

[a] A_z values reported in 10^{-4} cm^{-1}. [b] Percent deviation (PD) respect to the absolute experimental value calculated as: $100 \times [(|A_z|^{calcd} - |A_z|^{exptl})|/|A_z|^{exptl}]$.

3.9 Behavior of the systems $V^{IV}O^{2+}/L^x$/bipy and $V^{IV}O^{2+}/L^x$/phen in solution

The behavior of the systems $V^{IV}O^{2+}/\mathbf{L^1}$/bipy, $V^{IV}O^{2+}/\mathbf{L^1}$/phen, $V^{IV}O^{2+}/\mathbf{L^2}$/bipy and $V^{IV}O^{2+}/\mathbf{L^2}$/phen was examined in a mixture H_2O/DMSO 50/50 (v/v) as function of pH.

In **Figure 6** and **Figure S22**, the anisotropic EPR spectra measured in the systems $V^{IV}O^{2+}/\mathbf{L^1}$/bipy and $V^{IV}O^{2+}/\mathbf{L^1}$/phen are shown, while those recorded in the systems $V^{IV}O^{2+}/\mathbf{L^2}$/bipy and $V^{IV}O^{2+}/\mathbf{L^2}$/phen are reported in **Figures S23** and **S24**. At acidic pH values, the binary species of bipy and one ternary complex $V^{IV}O$–$\mathbf{L^1}$–bipy are formed in solution. In particular, $[VO(bipy)(H_2O)_3]^{2+}$ (with equatorial-equatorial coordination of bipy, indicated with **VII** in **Figure 6**) and $[VO(bipy)(H_2O)_3]^{2+}$ (equatorial-axial coordination of bipy, **VIII**) were revealed, the same species characterized in the system $V^{IV}O^{2+}$/bipy [76].

In addition to these binary species, the ternary complex $[VO(\mathbf{HL^1}\text{-}O_1^-,N_1,O_2)(bipy)]^+$ (**IX** in **Figure 6**) have also been detected. In this adduct, the ligand in the mono deprotonated form behaves as tridentate and occupies three of the four equatorial position, while 2,2'-bipyridine is an equatorial-axial arrangement. Its spectral parameters (g_z = 1.951 and A_z = 162.8 × 10^{-4} cm^{-1}) are different with respect to the 1:2 species of bipy, $[VO(bipy)_2(H_2O)]^{2+}$ (g_z = 1.957

and A_z = 162.1 × 10^{-4} cm^{-1} [76]). These results indicate that **L**^{1} cannot compete with 2,2'-bipyridine for $V^{IV}O^{2+}$ binding in the neutral form **H$_2$L**^{1} and that the keto and amide groups are less basic than the aromatic N donors. Only with the deprotonation, the ligand in the form (**HL**^{1})$^{-}$ or (**L**^{1})$^{2-}$ is able to bind vanadium and ternary $V^{IV}O$–**L**^{1}–bipy or binary $V^{IV}O$–**L**^{1} complexes appear in solution.

Around the neutrality, with the second deprotonation of **L**^{1}, [VO(**L**^{1})(bipy)] (**Ia**) and [VO(**L**^{1})(H_2O)] (**II**) are formed: they are the same species detected when the solid compound [VO(**L**^{1})(bipy)] is dissolved in an organic solution. The spin Hamiltonian parameters for [VO(**L**^{1})(bipy)] are g_z = 1.951 and A_z = 160.9 × 10^{-4} cm^{-1}, very similar to those measured in DMF/DMSO mixture (g_z = 1.950 and A_z = 160.3 × 10^{-4} cm^{-1}) and A_z is comparable with that predicted by DFT methods (157.5 × 10^{-4} cm^{-1}) with a PD below 3%, coherent with the data in the literature for $V^{IV}O$ complexes [54]. The relative intensity of the EPR resonances indicates that [VO(**L**^{1})(bipy)] is the major species in solution, whereas [VO(**L**^{1})(H_2O)] is only a minor complex. To confirm this finding, the relative stability of these two compounds was determined by DFT methods and ΔE_{aq} and ΔG_{aq} for the reaction [VO(**L**^{1})(H_2O)] + bipy ⇄ [VO(**L**^{1})(bipy)] + H_2O was calculated. The results show that the hexa-coordinated complex [VO(**L**^{1})(bipy)] is much more stable than [VO(**L**^{1})(H_2O)], in agreement with what was observed with EPR spectroscopy, and that the difference in stability increases from gas phase to aqueous solution (**Table 7**).

Table 7. Calculated ΔE and ΔG for the formation in aqueous solution of the ternary species [$V^{IV}O$(**L**^{1})(bipy)], [$V^{IV}O$(**L**^{1})(phen)] and [VO(**L**^{1})(MeIm)].[a]

Reaction	ΔE_{aq} [b]	ΔG_{aq} [b]
[VO(**L**^{1})(H_2O)] + bipy ⇄ [VO(**L**^{1})(bipy)] + H_2O	-8.2	-5.0

[VO(**L**^{1})(H_2O)] + phen ⇄ [VO(**L**^{1})(phen)] + H_2O	-7.0	-2.6
[VO(**L**^{1})(H_2O)] + MeIm ⇄ [VO(**L**^{1})(MeIm)] + H_2O	-5.3	-4.3
[VO(**L**^{1})(bipy)] + MeIm ⇄ [VO(**L**^{1})(MeIm)] + bipy	2.9	0.7
[VO(**L**^{1})(phen)] + MeIm ⇄ [VO(**L**^{1})(MeIm)] + phen	1.7	-1.7

[a] Calculations carried out with SMD continuum model for water using the functional B3P86 and the basis set 6-311g. [b] Values reported in kcal mol^{-1}.

In the basic pH range OH^- ion replaces bipy ligand in the coordination sphere of $V^{IV}O^{2+}$ ion and [VO(**L**^{1})(bipy)] transforms into [VO(**L**^{1})(OH)]$^-$ (**III** in **Figure 6**), analogous to the species revealed in the binary system $V^{IV}O^{2+}$/**L**^{1}.

The experimental and calculated by DFT methods spin Hamiltonian parameters for mixed $V^{IV}O$ complexes formed by bipy and phen with **L**^{1} are reported in **Table 8**, while the optimized structures in **Figure 7**.

EPR spectra of the $V^{IV}O^{2+}$/**L**^{1}/phen system in the mixture H_2O/DMSO 50/50 (v/v) are shown in **Figure S22**. The behavior is comparable to that of the ternary system $V^{IV}O^{2+}$/**L**^{1}/bipy. The only significant difference is the higher stability of [VO(**L**^{1})(phen)] than [VO(**L**^{1})(bipy)], suggested by the absence of the species [VO(**L**^{1})(H_2O)] in the systems with phen (cfr. the spectra recorded at pH 8.60 in **Figures 7** and **Figure S22**) and by the pH value at which [VO(**L**^{1})(OH)]$^-$ appears in solution (around 11 in the system with phen and 10 in that with bipy).

The spin Hamiltonian parameters measured in the mixture H_2O/DMSO for [VO(**L**^{1})(phen)] (g_z = 1.951 and A_z = 160.8 × 10^{-4} cm^{-1}) are similar to those extracted in DMF/DMSO (g_z = 1.951 and A_z = 160.2 × 10^{-4} cm^{-1}).

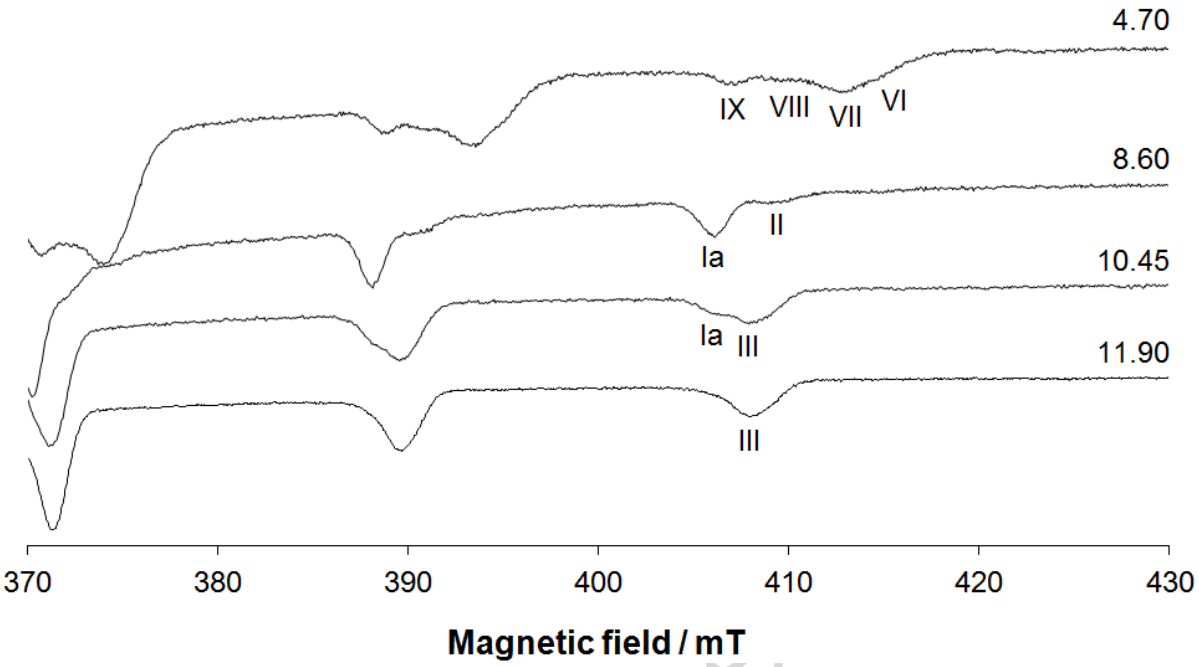

Figure 6. High field region of the X-band anisotropic EPR spectra (120 K) recorded in a mixture H_2O/DMSO 50/50 (v/v) as a function of pH in the system $V^{IV}O^{2+}$/**L**^{1}/bipy with a molar ratio of 1:1:1 and V concentration of 1.0×10^{-3} M. With **Ia**, **II**, **III**, **VI**, **VII**, **VIII** and **IX** are indicated the M_I = 7/2 resonances of the species [VO(**L**^{1})(bipy)], [VO(**L**^{1})(H_2O)], [VO(**L**^{1})(OH)]$^{-}$, [VO(H_2**L**^{1}-O_1,N_1)(H_2O)$_2$]$^{2+}$, [VO(bipy)((H_2O)$_3$]$^{2+}$ (equatorial-equatorial coordination), [VO(bipy)((H_2O)$_3$]$^{2+}$ (equatorial-axial coordination) and [VO(H**L**^{1}-O_1^{-},N_1,O_2)(bipy)]$^{+}$.

Table 8. Experimental (exptl) and DFT calculated (calcd) spin Hamiltonian parameters for ternary $V^{IV}O$ complexes formed by **L**^{1}, **L**^{2}, bipy and phen in H_2O/DMSO 50/50 (v/v) solution.[a]

Complex	g_z^{exptl}	A_z^{exptl}	A_z^{calcd}	PD [b]
[VO(H**L**^{1}-O_1^{-},N_1,O_2)(bipy)]$^{+}$	1.951	162.8	160.4	-1.5
[VO(H**L**^{1}-O_1^{-},$N1$,O_2)(phen)]$^{+}$	1.951	162.6	160.2	-1.5
[VO(**L**^{1})(bipy)]	1.950	160.9	157.5	-2.1

[VO(**L**^{1})(phen)]	1.951	160.8	157.1	-2.3
[VO(H**L**^{2}-O_1^-,N_1,O_2)(bipy)]$^{+}$	1.951	162.4	160.4	-1.2
[VO(H**L**^{2}-O_1^-,N_1,O_2)(phen)]$^{+}$	1.951	162.3	160.2	-1.3
[VO(**L**^{2})(bipy)]	1.951	160.6	157.5	-1.9
[VO(**L**^{2})(phen)]	1.951	161.4	157.1	-2.7

[a] A_z values reported in 10^{-4} cm^{-1}. [b] Percent deviation (PD) respect to the absolute experimental value calculated as: $100 \times [(|A_z|^{calcd} - |A_z|^{exptl})|/|A_z|^{exptl}]$.

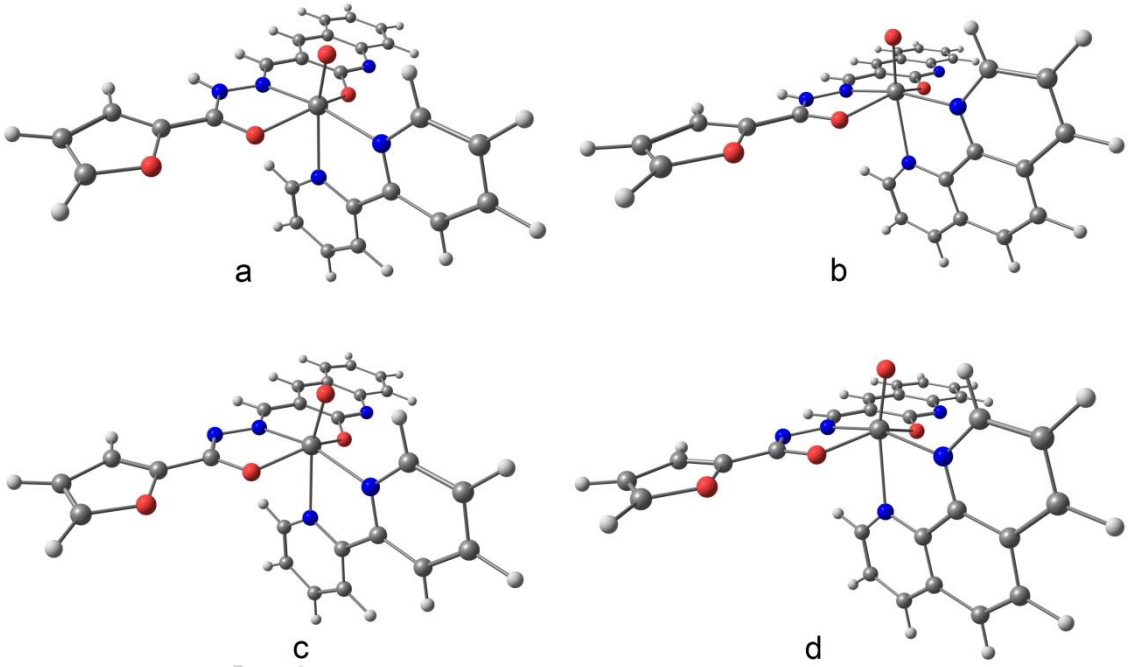

Figure 7. Optimized structures of the ternary $V^{IV}O$ complexes formed by **L**^{1} with bipy and phen in H_2O/DMSO mixtures: (a) [VO(H**L**^{1}-O_1^-,N_1,O_2)(bipy)]$^{+}$; (b) [VO(H**L**^{1}-O_1^-,N_1,O_2)(phen)]$^{+}$; (c) [VO(**L**^{1})(bipy)]; (d) [VO(**L**^{1})(phen)].

3.10 Behavior of the systems $V^{IV}O^{2+}$/$\mathbf{L}^{x}$/MeIm and [VO($\mathbf{L}^{x}$)(bipy/phen)]/protein in solution

To examine the possible binding of the complexes [VO($\mathbf{L}^{x}$)(bipy)] and [VO($\mathbf{L}^{x}$)(phen)] with proteins, the ternary systems $V^{IV}O^{2+}$/$\mathbf{L}^{1}$/MeIm and $V^{IV}O^{2+}$/$\mathbf{L}^{2}$/MeIm, where MeIm is 1-methylimidazole, were studied. Only the EPR spectra recorded in the first system are shown in **Figure 8**, the behavior of the second system being very similar. 1-Methylimidazole is a good model for the protein binding with a histidine (His) nitrogen [29a-b,30b-c], and can replace, around physiological pH, the water molecule in the equatorial position in a species as [VO($\mathbf{L}^{x}$)(H_2O)], forming [VO($\mathbf{L}^{x}$)(MeIm)] and shifting toward right the equilibrium [VO($\mathbf{L}^{x}$)(bipy/phen)] + H_2O ⇄ [VO($\mathbf{L}^{x}$)(H_2O)] + bipy/phen. This has been demonstrated for bis-chelated $V^{IV}O$ complex formed by 1-2-dimethyl-3-hydroxy-4(1*H*)-pyridinone (dhp), for which in aqueous solution the equilibrium $[VO(dhp)_2]$ + H_2O ⇄ $[VO(dhp)_2(H_2O)]$ exists, that is shifted toward right upon the binding of 1-methylimidazole [29a-c,29g-h].

From an examination of **Figure 8**, it can be noted that around pH 8 the resonances of the species [VO($\mathbf{L}^{1}$)(H_2O)] (indicated with **II**) are replaced by those of [VO($\mathbf{L}^{1}$)(MeIm)] (indicated with **X**). The value of A_z decreases from 167.2 × 10^{-4} cm^{-1} to 163.4 × 10^{-4} cm^{-1}, in good agreement with what is expected on the basis of the 'additivity relationship' [55]. DFT calculations predict, both for [VO($\mathbf{L}^{1}$)(MeIm)] and [VO($\mathbf{L}^{2}$)(MeIm)], a value of A_z practically coincident with the experimental one (**Table 9**). The value of ΔG_{aq} for the reaction [VO($\mathbf{L}^{1}$)(H_2O)] + MeIm ⇄ [VO($\mathbf{L}^{1}$)(MeIm)] + H_2O is -4.3 kcal mol^{-1}, while that for the reactions [VO($\mathbf{L}^{1}$)(bipy/phen)] + H_2O ⇄ [VO($\mathbf{L}^{1}$)(H_2O)] + MeIm ⇄ [VO($\mathbf{L}^{1}$)(MeIm)] + bipy/phen is 0.7 and -1.7 kcal mol^{-1}, respectively (see **Table 7**). These data appear to be consistent with the possibility of formation of [VO($\mathbf{L}^{x}$)(MeIm)] in aqueous solution and suggest that, in principle, a protein could replace the water or bipy/phen ligand in [VO($\mathbf{L}^{x}$)(H_2O)] or [VO($\mathbf{L}^{x}$)(bipy/phen)] to form adducts with composition [VO($\mathbf{L}^{x}$)]$_n$(Protein), where *n* is the number of VO$\mathbf{L}^{x}$ moieties that interact with the accessible

residues of protein, which can be His but also Asp or Glu, as demonstrated recently in the literature [77]. The two optimized structures of [VO(**L**^{1})(MeIm)] and [VO(**L**^{2})(MeIm)] are reported in **Figure S25**.

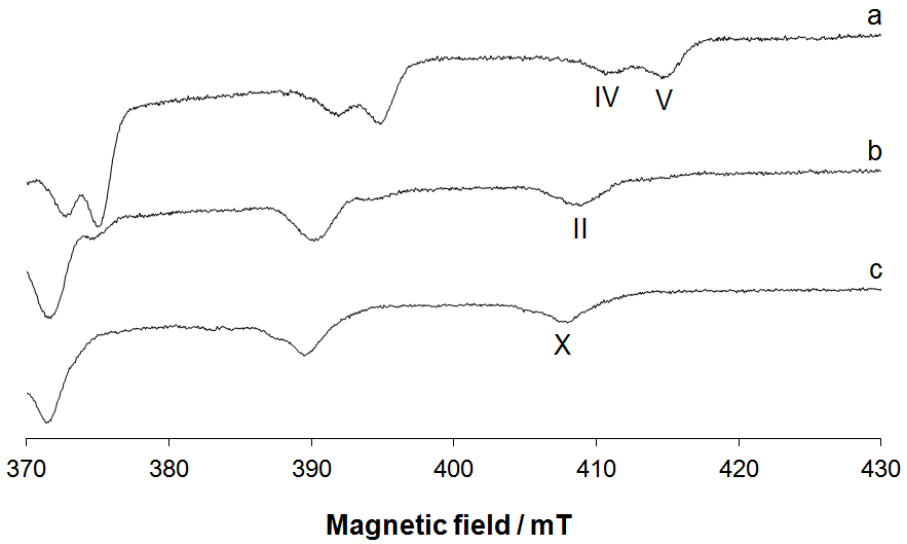

Figure 8. High field region of the X-band anisotropic EPR spectra (120 K) recorded in a mixture H_2O/DMSO 50/50 (v/v) as a function of pH in the system $V^{IV}O^{2+}$/**L**^{1} and $V^{IV}O^{2+}$/**L**^{1}/MeIm with a V concentration of 1.0 × 10^{-3} M. a) $V^{IV}O^{2+}$/**L**^{1} 1:1 at pH 6.60; b) $V^{IV}O^{2+}$/**L**^{1} 1:1 at pH 8.85; c) $V^{IV}O^{2+}$/**L**^{1}/MeIm 1:1:4 at pH 8.65. The M_I = 7/2 resonances of the species [VO(**L**^{1})(H_2O)] (**II**), [VO(H**L**^{1}-O_1^{-},N_1,O_2)(H_2O)]$^{+}$ (**IV**), [VO(H**L**^{1}-O_1^{-},N_1)(H_2O)$_2$]$^{+}$ (**V**) and [VO(**L**^{1})(MeIm)] (**X**) are indicated.

Table 9. Experimental (exptl) and DFT calculated (calcd) parameters for the mixed $V^{IV}O$ complexes with MeIm in a mixture H_2O/DMSO.[a]

Complex	g_z^{exptl}	A_z^{exptl}	A_z^{calcd}	PD [b]
[VO(**L**^{1})(MeIm)] (**X**)	1.949	163.4	163.5	0.0
[VO(**L**^{2})(MeIm)]	1.950	163.2	163.3	0.0

[a] A_z values reported in 10^{-4} cm^{-1}. [b] Percent deviation (PD) from the absolute experimental value calculated as: $100 \times [|(|A_z|^{calcd} - |A_z|^{exptl})|/|A_z|^{exptl}]$.

Lysozyme (Lyz) and cytochrome *c* (Cyt) are two of the most frequently used model proteins to study the interactions with the potential metallodrugs by mass spectrometry techniques [78]. In this paper the interaction of [VO(**L**^{1})(bipy)] (**1**) and [VO(**L**^{1})(phen)] (**2**) with Lyz and Cyt was examined with a view to evaluate the biological activity of these $V^{IV}O$ species and their binding to the serum proteins. Lysozyme is a protein formed of 129 amino acids (14300 Da) and its relatively small size renders it suitable for ESI-MS studies. In its structure only one His residue exists (His15) and it is very likely that this represents a general binding site for some transition metal complexes [78]. The positive ESI-MS spectrum of lysozyme is characterized by a series of well-resolved peaks in the m/z range 1100-1800 with a charge distribution from z = 8 to z = 13 (**Figure 9a**) [79].

The ESI-MS spectra on the system [VO(**L**^{1})(bipy/phen)]/Lyz were recorded using two different protein concentrations (5 and 50 μM) and different metal-to-protein ratio (3/1 and 5/1). The results obtained were similar for both complexes. As an example, in **Figure 9a** the spectra obtained in the range 200-2000 m/z for the system [VO(**L**^{1})(phen)]/Lyz 3/1 with a protein concentration of 5 μM are reported.

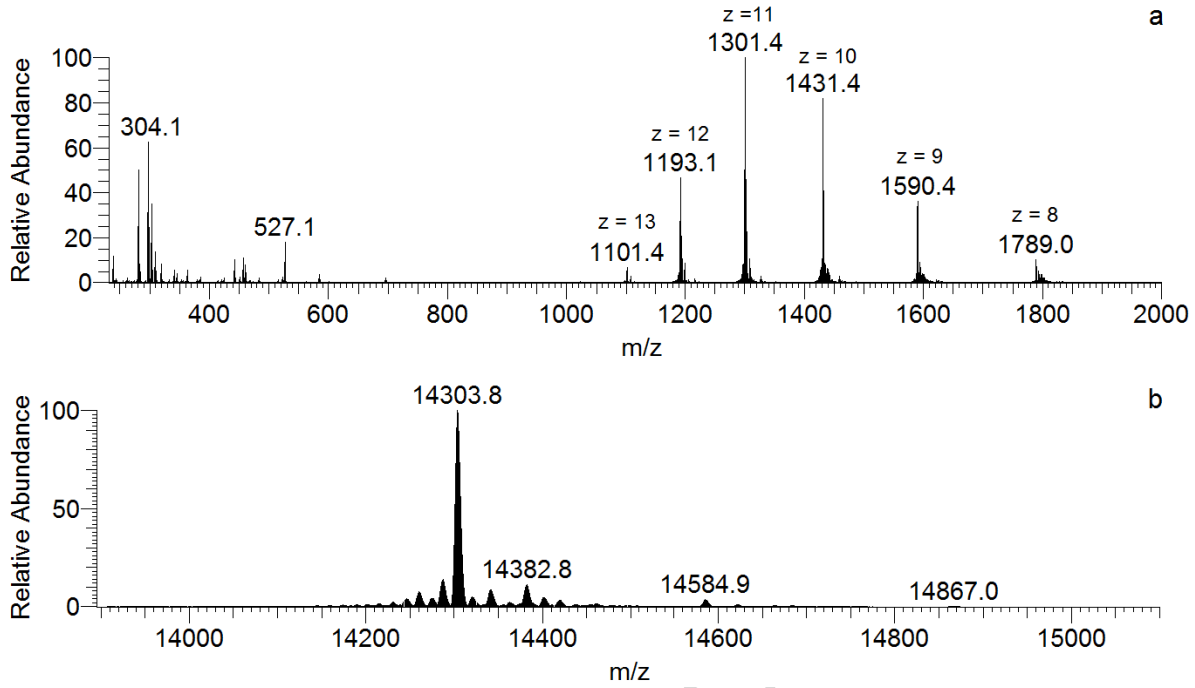

Figure 9. a) ESI-MS spectrum recorded on the system containing [VO(**L**^{1})(phen)] and lysozyme (5 μM) with a molar ratio of 3/1; a) signal obtained in the range 200-2000 m/z and b) deconvoluted signal.

To determine the exact mass of the adducts, the spectra were deconvoluted with the Xtract software and that measured with a molar ratio [VO(**L**^{1})(phen)]/Lyz of 3/1 and lysozyme concentration of 5 μM is reported in **Figure 9b**; similar results are obtained with a ratio [VO(**L**^{1})(phen)]/Lyz of 5/1. It can be noticed a central intense peak at 14303.8 Da – which corresponds to the mass of the free protein – with a series of other signals due to the adducts with a different number of Na^{+} ions (23 Da) and/or H_2O molecules (18 Da). Each peak is also split in several signals, due to the different isotopic distribution of the revealed species. In addition to the peak of the free protein, the signals at 14584.9 and 14867.0 Da are revealed, which can be attributed to the species [H_2**L**^{1}]–Lyz and {2[H_2**L**^{1}]}–Lyz, where one or two ligand molecules (with mass of 282 Da) are bound to the protein. Another peak with a lower

intensity is detected at 14382.8 Da, which belongs to the protein adduct with DMSO (i.e., the solvent used to dissolve $V^{IV}O$ complex with a mass of 79 Da).

In the m/z range 200-600, the peak attributable to the adducts $[VO(\mathbf{L^1})(phen)]+H]^+$ at m/z 527.1 is observed with high intensity; the comparison between the simulated isotopic pattern and the experimental spectrum is reported in **Figure S26**.

Similarly to lysozyme, cytochrome *c* shows features suitable to be studied by ESI-MS technique; in fact, it is a rather small protein (104 amino acids and molar mass < 12400 Da) and presents a well-resolved spectrum in the m/z range 1000–2000 [80]. The most important sites should be His26 and His33 (i.e. the two histidine residues not bound to iron) [80]. Interestingly, the spectra recorded in the systems $[VO(\mathbf{L^1})(\mathbf{L^{N-N}})]$/Cyt gave similar results to those with Lyz and no adducts ascribable to the binding of VO–$\mathbf{L^1}$ or VO–$\mathbf{L^1}$–bipy/phen with cytochrome *c* were detected. Only the signals of the free complexes $[VO(\mathbf{L^1})(phen)]+H]^+$ and $[VO(\mathbf{L^1})(bipy)]+H]^+$ at m/z = 527.1 Da and m/z = 503.1 Da were observed.

The results suggest that there is no interaction between $V^{IV}O$ species and the two proteins examined. This can be explained with the low number of accessible coordinating and polar residues, which preclude the covalent binding through the formation of one or more coordination bonds and non-covalent interaction through hydrogen or van der Waals contacts. In fact as demonstrated in two recent papers, the binding is also governed by the relative exposition of the possible donors of the protein and secondary that could stabilize the adducts [77,81].

3.11 Fluorescence quenching studies of Bovine Serum Albumin

The binding of metal complexes with BSA is generally studied through fluorescence quenching method [45]. Fluorescence in BSA is brought about by two intrinsic moieties of the protein, viz. tryptophan and tyrosine [67]. Interactions such as energy transfer, ground-

state complex formation, and also protein conformational transitions, subunit associations, substrate binding, or denaturation are caused by the changes in the emission spectra of tryptophan moiety of BSA. Hence, BSA is frequently selected as a model protein to study the influence of metal complexes on serum proteins [82].

Interaction of the complexes **1-8** with BSA protein was investigated through fluorescence measurements. Herein, spectra were recorded by titrating BSA (10 µM) with increasing concentration of the complexes (0–100 µM) in the range of 305–500 nm upon excitation at 295 nm. The addition of increasing concentrations of the complexes **1-8** to BSA leads to changes in its fluorescence emission spectra. The representative emission spectra of the complexes **7** and **8** are shown in **Figure 10** and the rest of spectrums (**1**–**6**) are given in **Figures S27**–**S32**. It was observed that there is appreciable decrease in the fluorescence intensity of BSA around 347 nm for all the complexes with a blue shift of around 4 to 6 nm. While there was a gradual quench in the tryptophan fluorescence intensity of BSA on increasing the concentration for all the complexes, complex **7** showed a drastic decrease in the fluorescence intensity, which revealed that the binding affinity of **7** is higher than other complexes towards BSA.

This fluorescence quenching can be further studied by the Stern–Volmer relationship as shown in Eq. 1 and can be expressed in terms of bimolecular quenching rate constant and average life time of the fluorophore:

$$\frac{Fo}{F} = 1 + k\mathrm{q}\,\tau_o\,[\mathrm{Q}] = 1 + \mathrm{Ksv}[\mathrm{Q}] \qquad (1)$$

where F_0 and F are the fluorescence intensities in the absence and the presence of a quencher (i.e. complex **1**−**8**) respectively, k_q is the bimolecular quenching rate constant, τ_0 is the average life time of fluorophore in the absence of a quencher and [Q] is the concentration of a quencher. K_{SV} is the Stern–Volmer quenching constant in M^{-1}. The binding constant (K_a) and number of binding site (*n*) was calculated from the Scatchard equation Eq. 2:

$$\log \frac{Fo-F}{F} = \log Ka + n \log[Q] \qquad (2)$$

Table 10 shows data from Stern-Volmer and Scatchard plots. The results indicate that the quenching constants for **7** and **8** were found to be 1.0×10^5 and 4.5×10^4 M^{-1}, respectively, which shows that the quenching ability of **7** and **8** is higher than other complexes. The quenching constant of the complexes are in the order of **7** > **8** > **4** > **6** > **2** > **5**> **3**> **1** (**Table 10** and **Figure 10**). The degree of quenching of the fluorescence intensity provides an insight into the extent of interaction of metal complexes with BSA. Additionally, the binding constant of **7** (5.0×10^5 M^{-1}) and **8** (1.3×10^5 M^{-1}) were found to be better in comparison to other complexes, while the binding constant of others complexes showed a similar pattern as observed for the quenching constant (**Table 10** and **Figure 10**). Furthermore, metal complexes bind independently to a set of sites in a protein moiety and the number of binding site observed for this series of complexes was also higher for complexes **7** and **8** (**Table 10**). The presence of an extra electron-donating substituent (−OH group) in the ligand environment of complexes (**7** and **8**), which is also able to form hydrogen bonds with BSA surface residues, can be a probable reason for their enhanced binding affinity towards BSA in comparison to other complexes, which is clearly reflected in their K_a value (**Table 10**).

Table 10. BSA binding parameters of complex **1** – **8**.

Complex	Stern–Volmer Constant K_{sv} (M^{-1})	Bimolecular rate constant k_q (M^{-1} s^{-1})	Binding Constant K_a (M^{-1})	Number of binding sites (n)
1	9.7×10^3	1.5×10^{12}	3.9×10^2	0.60
2	1.4×10^4	2.1×10^{12}	2.5×10^3	0.80
3	1.1×10^4	1.9×10^{12}	1.2×10^3	0.75

4	1.7×10^4	2.8×10^{12}	3.9×10^3	0.80
5	1.3×10^4	2.2×10^{12}	1.4×10^3	0.76
6	1.6×10^4	2.6×10^{12}	3.4×10^3	0.83
7	1.0×10^5	1.6×10^{13}	5.0×10^5	1.17
8	4.5×10^4	7.2×10^{12}	1.3×10^5	1.11

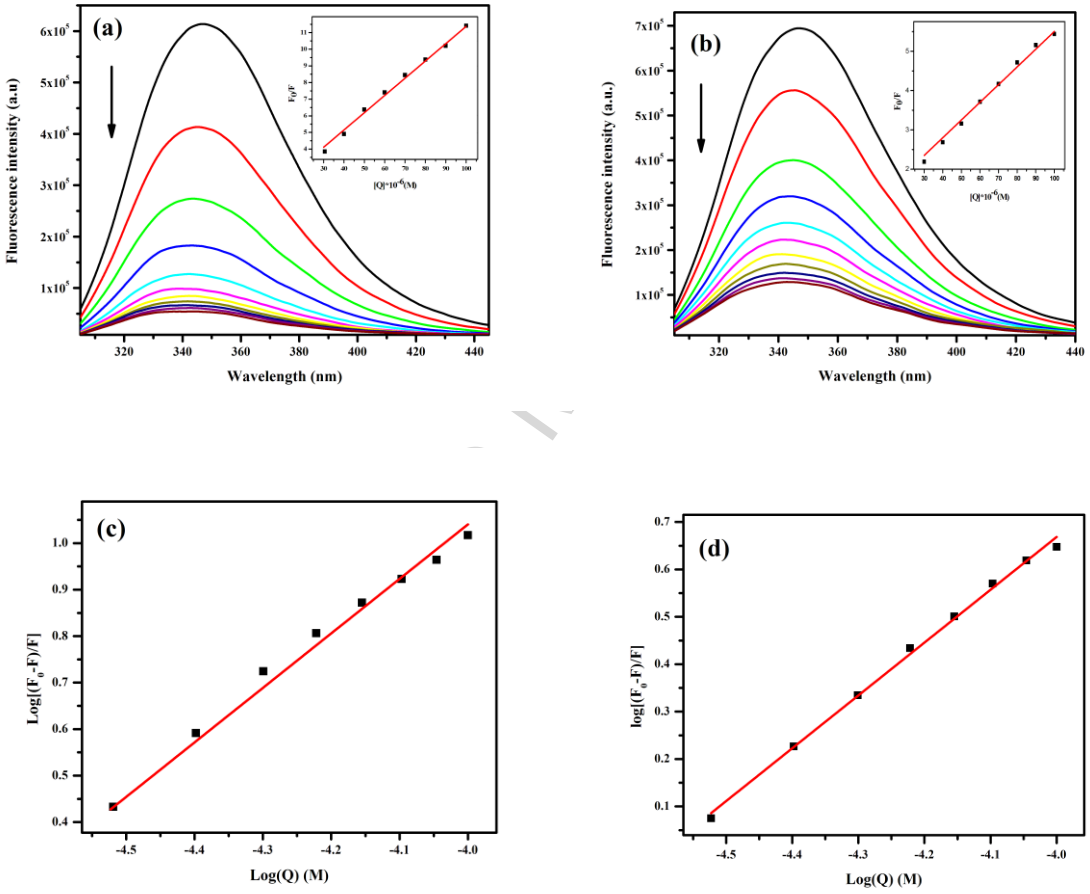

Figure 10. (a) Fluorescence quenching of BSA (10 µM) by complex [$V^{IV}O$(**L**^{4})(bipy)] (**7**) (0–100 µM) and the inset shows the Stern-Volmer plot of complex [$V^{IV}O$(**L**^{4})(bipy)] (**7**); (b) Fluorescence quenching of BSA(10 µM) by complex [$V^{IV}O$(**L**^{4})(phen)] (**8**) (0–100 µM) and the inset shows the Stern-Volmer plot of complex [$V^{IV}O$(**L**^{4})(phen)] (**8**); (c) Scatchard plot of complexes [$V^{IV}O$(**L**^{4})(bipy)] (**7**) and (d) Scatchard plot of complexes [$V^{IV}O$(**L**^{4})(phen)].

3.12 DNA binding studies

Absorption spectroscopic studies

The binding affinity of the complexes towards CT-DNA was examined through absorption spectroscopic technique. The complexes gave absorption bands in the range 401–300 nm for the LMCT and intra-ligand transitions respectively. On gradual addition of CT-DNA, the absorption bands due to the aforementioned transitions showed a hypochromic shift for all the complexes (**Figures 11** and **S33**). This hypochromic shift may be attributed to the association of the DNA bases with the electronic states of the chromophores present in the metal complexes. Furthermore, from these experiments the equilibrium binding constant (Kb) of the complexes towards CT-DNA was determined (**Table 11** and **Figures 11** and **S33**) by following the Eq. 3.

$$\frac{[DNA]}{\varepsilon_a - \varepsilon_f} = \frac{[DNA]}{\varepsilon_b - \varepsilon_f} + \frac{1}{K_b(\varepsilon_b - \varepsilon_f)} \qquad (3)$$

Where [DNA] stands for the concentration of DNA base pairs, and ε_a, ε_f and ε_b correspond to apparent extinction coefficients for the complex i.e. Abs/[complex] in the presence of DNA, in the absence of DNA and to fully bound DNA respectively. A plot of [DNA]/($\varepsilon_a - \varepsilon_f$) vs. [DNA] gave a slope and the intercept equal to 1/($\varepsilon_b - \varepsilon_f$) and 1/$K_b$($\varepsilon_b - \varepsilon_f$), respectively, and the binding constant K_b was calculated from the ratio of the slope to the intercept. From the K_b values, it was deduced that the complexes showed binding affinity in the range of 10^3–10^4 M^{-1}, while the order of DNA binding propensity was found to be **7** > **8** > **4** > **6** > **2** > **5**> **3**> **1** (**Table 11**). This is almost identical to the order of binding constant of the relative complexes with BSA as observed before; with an exception of complex **8** and **4** being near about similar in terms of their K_b value. This higher binding affinity of complex **7** and **8** may be attributed to the presence of extra electron-donating substituent (−OH group) in the ligand backbone with comparison to rest of the complexes [83,84], which is clearly reflected in their K_b value

(**Table 11**). Also, the ligands revealed binding affinity to CT-DNA significantly lower than their corresponding complexes.

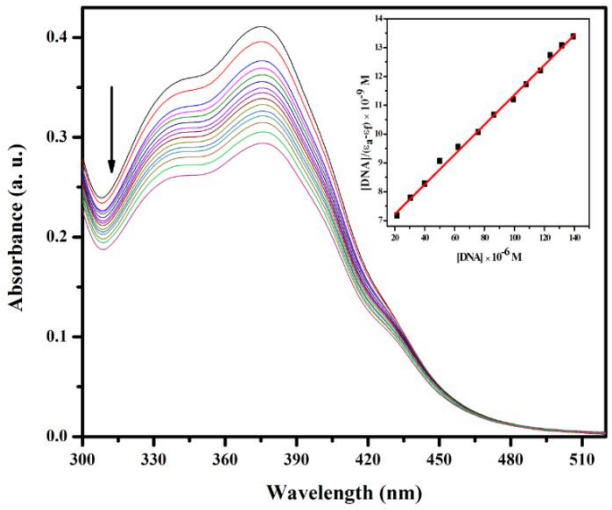

Figure 11. Electronic absorption spectra of [$V^{IV}O(\mathbf{L}^4)$(bipy)] (**7**) (25 μM) upon the titration of CT-DNA (0–150 μM) in 50 mM Tris-HCl buffer at pH 8.0. Arrow shows the decrease in absorbance with respect to an increase in the CT-DNA concentration. The inset shows the linear fit of [DNA]/($\varepsilon_a - \varepsilon_f$) vs. [DNA].

Table 11. CT-DNA binding parameters with complex **1** – **8**.

Complex	BindingConstant (K_b)[a] (M^{-1})	Bimolecular rate constant (k_q)[b] (M^{-1} s^{-1})
[$V^{IV}O(\mathbf{L}^1)$(bipy)] **(1)**	8.20×10^3	3.4×10^{12}
[$V^{IV}O(\mathbf{L}^1)$(phen)] **(2)**	1.04×10^4	1.3×10^{12}
[$V^{IV}O(\mathbf{L}^2)$(bipy)] **(3)**	8.73×10^3	1.2×10^{12}
[$V^{IV}O(\mathbf{L}^2)$(phen)] **(4)**	1.15×10^4	4.0×10^{12}
[$V^{IV}O(\mathbf{L}^3)$(bipy)] **(5)**	9.45×10^3	4.6×10^{12}

$[V^{IV}O(\mathbf{L}^3)(phen)]$ **(6)**	1.10×10^4	3.2×10^{12}
$[V^{IV}O(\mathbf{L}^4)(bipy)]$ **(7)**	1.38×10^4	5.0×10^{12}
$[V^{IV}O(\mathbf{L}^5)(phen)]$ **(8)**	1.18×10^4	2.1×10^{12}

[a] DNA binding constants were determined by the UV-vis spectral method. [b] Bimolecular rate constant were determined through comparative fluorescence spectroscopic study.

In order to understand the binding mode of the complexes with CT-DNA, displacement assay or competitive binding experiment with fluorescent dye i.e. ethidium bromide (EB) was performed. EB is a DNA intercalating agent [45,67]. Generally, there is an increase in the quantum yield of the of EB upon binding with DNA, which leads to enhanced fluorescence [85,86]. However, when metal complexes interact with DNA through intercalation mode, they displace EB molecules and yield lower fluorescence intensity. In the present study, we find that all the complexes effectively displace EB molecules leading to decrease in fluorescence intensity (**Figures 12** and **S34**). Further, the k_q values and binding constant (Kb) for the complexes were obtained from the classical Stern–Volmer and Scatchard equation respectively and were found to be in the range $1.2\times10^{12} - 5.0\times10^{12}$ M^{-1} s^{-1} and $8.20\times10^{3} - 1.38\times10^{4}$ M^{-1}respectively (**Table 11**).

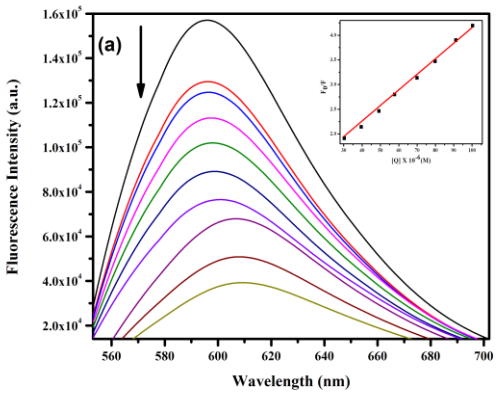

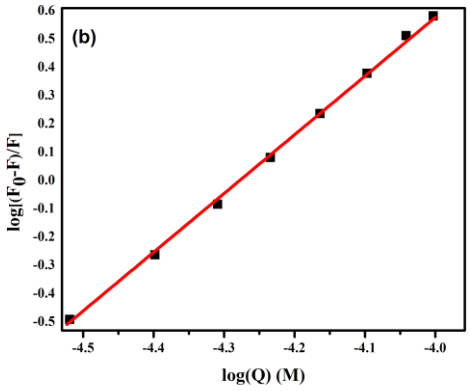

Figure 12. (a) Fluorescence quenching of EB (10 μM) upon the titration of complex [$V^{IV}O(\mathbf{L^4})$(bipy)] (**7**) (0–100 μM). Arrow shows the decrease in Fluorescence intensity with respect to an increase in the complex concentration and the inset shows the Stern-Volmer plot of [$V^{IV}O(\mathbf{L^4})$(bipy)] (**7**); (b) Scatchard plot of complexes [$V^{IV}O(\mathbf{L^4})$(bipy)] (**7**).

4. Conclusions

Four biologically active aroylhydrazone ligands with quinoline scaffold containing ONO donor sites have been prepared and used in the synthesis of a series of eight mononuclear oxidovanadium(IV) [$VO(\mathbf{L}^{x})(\mathbf{L}^{N\text{-}N})$] (**1-8**) complexes with the presence of *N*,*N*-donor bases like bipy (**1**, **3**, **5** and **7**) and phen (**2**, **4**, **6** and **8**). The complexes [$VO(\mathbf{L}^{x})(\mathbf{L}^{N\text{-}N})$] (**1-8**) were characterized through several spectroscopic techniques. The single-crystal XRD studies of **1** and **6** revealed the presence of a distorted octahedral geometry with the tridentate dianionic $\mathbf{L}^{x}$ in the *meridional* arrangement and bidentate bipy or phen with an equatorial-axial coordination. In order to study the interactions with proteins of these synthesized complexes, the behavior of the systems $V^{IV}O^{2+}/\mathbf{L}^{x}$, $V^{IV}O^{2+}/\mathbf{L}^{x}$/bipy and $V^{IV}O^{2+}/\mathbf{L}^{x}$/phen was examined as function of pH in a mixture of H_2O/DMSO 50/50 (v/v). DFT calculations revealed the relative stability of the tautomeric forms of the ligands, predicted the structure of V complexes and EPR parameters could be applied successfully to similar systems. Further, the studies of the interaction with the two model proteins, lysozyme and cytochrome *c*, revealed no interaction with [$VO(\mathbf{L}^{x})(\mathbf{L}^{N\text{-}N})$] complex. This is in contrast with evidences found in the literature for $V^{IV}O$ species with an accessible equatorial coordination – as the moieties $VO(\mathbf{L}^{x})$ – which are bound by His or Asp/Glu residues. Additionally, the interaction of the complexes with bovine serum albumin was also examined. These studies exhibited that the metal complexes showed higher affinity towards BSA in comparison to Lyz and Cyt. This could be explained with the higher number of accessible coordinating and polar residues for

BSA than for Lyz and Cyt. While all the complexes exhibited moderate BSA binding results, **7** and **8** were revealed to be the best among the series with Stern–Volmer quenching constant value of 10^5 M^{-1}, which can be attributed to the presence in the ligand environment of an electron-donating substituent (−OH group) that can also form hydrogen bonds with BSA surface residues. Experimental result also depicts that all the complexes shows moderate binding affinity towards CT-DNA and with coherence with the BSA interaction studies, complexes **7** and **8** also shows good binding affinity towards DNA in the range of $1.18 \times 10^4 - 1.38 \times 10^4$ M^{-1}, probably the presence of extra electron-donating substituent (−OH group) in the ligand backbone. In view of the above results, it can be anticipated that the present set of complexes may have the potential to stimulate further research towards the development of metal based agents for anticancer drugs.

Abbreviations

bipy	2,2′-bipyridine
phen	1,10-phenanthroline
BMOV	Bis(maltolato)oxidovanadium(IV)
BEOV	Bis(ethylmaltolato)oxidovanadium(IV)
Lyz	Lysozyme
Cyt	Cytochrome *c*
BSA	Bovine serum albumin
CT-DNA	Calf Thymus DNA
EB	Ethidium bromide
MeIm	1-Methylimidazole
ESI-MS	ElectroSpray Ionization Mass Spectroscopy

$VO(acac)_2$	Vanadyl acetylacetonate
CH_3CN	Acetonitrile
DMSO	Dimethylsulfoxide
CH_2Cl_2	Dichloromethane
DMF	Dimethylformamide
EtOH	Ethanol
MeOH	Methanol
A_z	^{51}V hyperfine coupling constant along the z axis

Conflicts of interest

There are no conflicts to declare.

Acknowledgements

R.D thanks DBT, Govt. of India [Grant No. 6241 P112/RGCB/PMD/DBT/RPDA/2015] for funding this research. D.S., V.U., G.S. and E.G. thank Fondazione di Sardegna (project FDS15Garribba) and Regione Autonoma della Sardegna (grant RASSR79857) for the financial support. G.S. thanks also Spanish MINECO (grant CTQ2017-87889-P) and Generalitat de Catalunya (2017SGR1323) and the Universitat Autònoma de Barcelona for its support to his Ph.D.

Notes and references

Author Contributions

The manuscript was written through contributions of all authors.

Corresponding Authors

*E-mail: rupamdinda@nitrkl.ac.in (Rupam Dinda)

*E-mail: garribba@uniss.it (Eugenio Garribba)

ORCID

Daniele Sanna: 0000-0001-9299-0141

Giuseppe Sciortino: 0000-0001-9657-1788

Valeria Ugone: 0000-0002-2830-3869

Eugenio Garribba: 0000-0002-7229-5966

Rupam Dinda: 0000-0001-9452-7791

‡ Electronic supplementary information (ESI) available (Tables **S1**−**S3**, Figures **S1**−**S33**): CCDC reference numbers 1856634 (compound **1**), 1856633 (compound **6**). For ESI and crystallographic data in CIF format see DOI: XXXXX

References

[1] (a) D. Rehder, Coord. Chem. Rev. 182 (1999) 297–322. (b) D. Rehder, J. Inorg. Biochem. 80 (2000) 133–136.

[2] J. O. Nriagu, Adv. in Environ. Sci. Technol. 30 (1998) 1–24.

[3] (a) H. U. Meisch, H. Bielig, Basic Res. Cardiol. 75 (1980) 413–417. (b) E. J. Baran, Adv. Plant Physiology. 10 (2008) 357–372. (c) M. Anke, Anales de la Real Academia Nacional de Farmacia. 70 (2004) 961–999.

[4] (a) L. C. Jr., Cantley, L. Josephson, R. Warner, M. Yanagisawa, C. Lechene, G. Guidotti, J. Biol. Chem. 252 (1977) 7421–7423. (b) M. D. Morsy, H. A. Abdel-Razek, O. M. Osman, J. Physiol Biochem. 67 (2011) 61–69.

[5] (a) D. Rehder, G. Santoni, G. M. Licini, C. Schulzke, B. Meier, Coord. Chem. Rev. 237 (2003) 53–63 (b) W. Plass, Coord. Chem. Rev. 237 (2003) 205–212. (c) A. Butler, Coord. Chem. Rev. 187 (1999) 17–35.

[6] (a) J. J. R. Frausto da Silva, R. J. P. Williams (Eds.), The Biological Chemistry of the Elements, 2nd ed., Oxford University Press: Oxford, U.K. 2001. (b) W. Kaim and B. Schwederski (Eds.), Bioinorganic Chemistry: Inorganic Elements in the Chemistry of Life; John Wiley & Sons: Chichester, U. K. 1994.

[7] R. R. Eady, Coord. Chem. Rev. 237 (2003) 23–30.

[8] (a) D. Gambino, Coord. Chem. Rev. 255 (2011) 2193–2203. (b) J. C. Pessoa, I. Tomaz, Curr. Med. Chem. 17 (2010) 3701–3738. (c) J. C. Pessoa, S. Etcheverry, D. Gambino, Coord. Chem. Rev. 301–302 (2015) 24–48.

[9] I. E. Leon, J. F. Cadavid-Vargas, A. L. Di Virgilio, S. B. Etcheverry, Curr. Med. Chem. 24 (2017) 112–148.

[10] H. Sakurai, Y. Kojima, Y. Yoshikawa, K. Kawabe, H. Yasui, Coord. Chem. Rev. 226 (2002) 187–198.

[11] (a) V. G. Yuen, P. Caravan, L. Gelmini, N. Glover, J. H. McNeill, I. A. Setyawati, Y. Zhou, C. Orvig, J. Inorg. Biochem. 68 (1997) 109–116. (b) B. A. Reul, S. S. Amin, J.-P. Buchet, L. N. Ongemba, D. C. Crans, S. M. Brichard, Br. J. Pharmacol. 126 (1999) 467–477. (c) S. S. Amin, K. Cryer, B. Zhang, S. K. Dutta, S. S. Eaton, O. P. Anderson, S. M. Miller, B. A. Reul, S. M. Brichard, D. C. Crans, Inorg. Chem. 39 (2000) 406–416. (d) M. Rangel, A. Tamura, C. Fukushima, H. Sakurai, J. Biol. Inorg. Chem. 6 (2001) 128–132.

[12] (a) H. Sakurai, Y. Fujisawa, S. Fujimoto, H. Yasui, T. Takino, J. Trace Elem. Exp. Med. 12 (1999) 393–401. (b) J. Gätjens, B. Meier, Y. Adachi, H. Sakurai, D. Rehder, Eur. J. Inorg. Chem. (2006) 3575–3585. (c) M. T. Cocco, V. Onnis, G. Ponticelli, B. Meier, D. Rehder, E. Garribba, G. Micera, J. Inorg. Biochem. 101 (2007) 19–29. (d) H. Esbak, E.

A. Enyedy, T. Kiss, Y. Yoshikawa, H. Sakurai, E. Garribba, D. Rehder, J. Inorg. Biochem. 103 (2009) 590–600.

[13] H. Sakurai, K. Fujii, H. Watanabe, H. Tamura, Biochem. Biophys. Res. Commun. 214 (1995) 1095–1101.

[14] (a) D. Rehder, Future Med. Chem. 4 (2012) 1823–1837. (b) D. Rehder, Future Med. Chem. 8 (2016) 325–338.

[15] (a) Y. Wei, C. Zhang, P. Zhao, X. Yang, K. Wang, J. Inorg. Biochem. 105 (2011) 1081–1085. (b) D. Rehder, J. C. Pessoa, C. F. G. C. Geraldes, T. Kabanos, T. Kiss, B. Meier, G. Micera, L. Pettersson, M. Rangel, A. Salifoglou, I. Turel, D. Wang, J. Biol. Inorg. Chem. 7 (2002) 384–396. (c) M. Sutradhar, T. R. Barman, G. Mukherjee, M. Kar, S. S. Saha, M. G. B. Drew, S. Ghosh, Inorg. Chim. Acta. 368 (2011), 13–20. (d) A. R. Saltiel, C. R. Khan, Nature. 414 (2001) 799–806. (e) P. Noblía, E. J. Baran, L. Otero, P. Draper, H. Cerecetto, M. González, O. E. Piro, E. E. Castellano, T. Inohara, Y. Adachi, H. Sakurai, D. Gambino, Eur. J. Inorg. Chem. (2004) 322–328. (f) J. Nilsson, A. A. Shteinman, D. Rehder, E. Nordlander, J. Inorg. Biochem. 105 (2011) 1795–1800. (g) G. R. Willsky, L.-H. Chi, Z. Hu and D. C. Crans, Coord. Chem. Rev. 255 (2011) 2258–2269. (h) D. Rehder, Inorg. Chem. Commun. 6 (2003) 604–617. (i) M. N. Islam, A. A. Kumbhar, A. S. Kumbhar, M. Zeller, R. J. Butcher, M. B. Dusane, B. N. Joshi, Inorg. Chem. 49 (2010) 8237–8246. (j) S. I. Pillai, S. P. Subramanian, M. Kandaswamy, Eur. J. Med. Chem. 63 (2013) 109–117.

[16] (a) N. Domingues, J. Pelletier, C. G. Ostenson, M. M. C. A. Castro, J. Inorg. Biochem. 131 (2014) 115–122. (b) J. Pelletier, N. Domingues, M. M. C. A. Castro, C.-G. Östenson, J. Inorg. Biochem. 154 (2016) 29–34. (c) K. H. Thompson, J. H. McNeill and C. Orvig, Chem. Rev. 99 (1999) 2561–2571.

[17] K. H. Thompson, C. Orvig, Coord. Chem. Rev. 219–221 (2001) 1033–1053.

[18] Y. Shechter, I. Goldwaser, M. Mironchik, M. Fridkin, D. Gefel, Coord. Chem. Rev. 237 (2003) 3–11.

[19] K. H. Thompson, C. Orvig, J. Inorg. Biochem. 100 (2006) 1925–1935.

[20] K. Kawabe, Y. Yoshikawa, Y. Adachi, H. Sakurai, Life Sci. 78 (2006) 2860–2866.

[21] H. Sakurai, Y. Yoshikawa, H. Yasui, Chem. Soc. Rev. 37 (2008) 2383–2392.

[22] K. H. Thompson, C. Orvig, Vanadium compounds in the treatment of diabetes, in: H. Sigel, A. Sigel (Eds.), Met. Ions Biol. Syst, Marcel Dekker, New York. 41 (2004) 221–252.

[23] J. H. McNeill, V. G. Yuen, H. R. Hoveyda, C. Orvig, J. Med. Chem. 35 (1992) 1489–1491.

[24] K. H. Thompson, J. Lichter, C. LeBel, M.C. Scaife, J.H. McNeill and C. Orvig, J. Inorg. Biochem. 103 (2009) 554–558.

[25] K. H. Thompson, B. D. Liboiron, Y. Sun, K. D. Bellman, I. A. Setyawati, B. O. Patrick, V. Karunaratne, G. Rawji, J. Wheeler, K. Sutton, S. Bhanot, C. Cassidy, J. H. McNeill, V. G. Yuen, C. Orvig, J. Biol. Inorg. Chem. 8 (2003) 66–74.

[26] H. Yasui, K. Takechi, H. Sakurai, J. Inorg. Biochem. 78 (2000) 185–196.

[27] D. Rehder, in Interrelations between Essential Metal Ions and Human Diseases, ed. A. Sigel, H. Sigel and R. K. O. Sigel, Springer Science + Business Media, Dordrecht, ch. 5 (2013) 139–169.

[28] J. C. Pessoa, E. Garribba, M. F. A. Santos, T. Santos- Silva, Coord. Chem. Rev. 301–302 (2015) 49–86.

[29] (a) D. Sanna, G. Micera, E. Garribba, Inorg. Chem. 49 (2010) 174–187. (b) D. Sanna, P. Buglyó, G. Micera, E. Garribba, J. Biol. Inorg. Chem. 15 (2010) 825–839. (c) D. Sanna, G. Micera, E. Garribba, Inorg. Chem. 50 (2011) 3717–3728. (d) D. Sanna, L. Bíró, P. Buglyó, G. Micera, E. Garribba, Metallomics. 4 (2012) 33–36. (e) D. Sanna, V. Ugone,

G. Micera, E. Garribba, Dalton Trans. 41 (2012) 7304–7318. (f) D. Sanna, L. Bíró, P. Buglyó, G. Micera, E. Garribba, J. Inorg. Biochem. 115 (2012) 87–99. (g) D. Sanna, G. Micera, E. Garribba, Inorg. Chem. 52 (2013) 11975–11985. (h) D. Sanna, M. Serra, G. Micera, E. Garribba, Inorg. Chem. 53 (2014) 1449–1464. (i) D. Sanna, M. Serra, G. Micera, E. Garribba, Inorg. Chim. Acta. 420 (2014) 75–84. (j) D. Sanna, V. Ugone, L. Pisano, M. Serra, G. Micera, E. Garribba, J. Inorg. Biochem. 153 (2015) 167–177. (k) T. Koleša-Dobravc, E. Lodyga-Chruscinska, M. Symonowicz, D. Sanna, A. Meden, F. Perdih, E. Garribba, Inorg. Chem. 53 (2014) 7960–7976. (l) D. Sanna, V. Ugone, G. Micera, T. Pivetta, E. Valletta, E. Garribba, Inorg. Chem. 54 (2015) 8237–8250. (m) D. Sanna, V. Ugone, G. Micera, P. Buglyó, L. Biró, E. Garribba, Dalton Trans. 46 (2017) 8950–8967. (n) D. Sanna, V. Ugone, M. Serra, E. Garribba, J. Inorg. Biochem. 173 (2017) 52–65. (o) D. Sanna, J. Palomba, G. Lubinu, P. Buglyó, S. Nagy, F. Perdih, E. Garribba, J. Med. Chem. 62 (2019) 654–664.

[30] (a) G. R. Willsky, A. B. Goldfine, P. J. Kostyniak, J. H. McNeill, L. Q. Yang, H. R. Khan, D. C. Crans, J. Inorg. Biochem. 85 (2001) 33–42. (b) B. D. Liboiron, K. H. Thompson, G. R. Hanson, E. Lam, N. Aebischer, C. Orvig, J. Am. Chem. Soc. 127 (2005) 5104–5115. (c) B. D. Liboiron, in High Resolution EPR, ed. L. Berliner, G. Hanson, Springer, New York, 2009, ch. 12, 507-549. (d) T. Jakusch, D. Hollender, E. A. Enyedy, C. S. Gonzalez, M. Montes-Bayon, A. Sanz-Medel, J. C. Pessoa, I. Tomaz, T. Kiss, Dalton Trans. (2009) 2428–2437. (e) I. Correia, T. Jakusch, E. Cobbinna, S. Mehtab, I. Tomaz, N. V. Nagy, A. Rockenbauer, J. C. Pessoa, T. Kiss, Dalton Trans. 41 (2012) 6477–6487. (f) S. Mehtab, G. Gonçalves, S. Roy, A. I. Tomaz, T. Santos-Silva, M. F. A. Santos, M. J. Romão, T. Jakusch, T. Kiss, J. C. Pessoa, J. Inorg. Biochem. 121 (2013) 187–195. (g) G. Gonçalves, I. Tomaz, I. Correia, L. F. Veiros, M. M. C. A. Castro, F. Avecilla, L. Palacio, M. Maestro,T. Kiss, T. Jakusch, M. H. V. Garcia, J. C.

Pessoa, Dalton Trans. 42 (2013) 11841–11861. (h) M. F. A. Santos, I. Correia, A. R. Oliveira, E. Garribba, J. C. Pessoa, T. Santos-Silva, Eur. J. Inorg. Chem. (2014) 3293–3297.

[31] Y. Yoshikawa, H. Sakurai, D. C. Crans, G. Micera, E. Garribba, Dalton Trans. 43 (2014) 6965–6972.

[32] L. H. S. Á. Terra, M. C. da Cunha Areias, I. Gaubeur, M. Encarnación, V. Suárez-iha, Spectrosc. Lett. 32 (1999) 257–271.

[33] (a) M. R. Maurya, S. Agarwal, M. Abid, A. Azam, C. Bader, M. Ebel, D. Rehder, Dalton Trans. (2006) 937–947. (b) L. Savini, L. Chiasserini, V. Travagli, C. Pellerano, E. Novellino, S. Cosentino, M. B. Pisano, Eur. J. Med. Chem. 39 (2004) 113–122. (c) Z. Cui, X. Yang, Y. Shi, H. Uzawa, J. Cui, H. Dohi, Y. Nishida, Bioorg. Med. Chem. Lett. 21 (2011) 7193–7196.

[34] (a) J. Easmon, G. Puerstinger, K. S. Thies, G. Heinisch, J. Hofmann, J. Med. Chem. 49 (2006) 6343–6350. (b) T. B. Chaston, R. N. Watts, J. Yuan, D. R. Richardson, Clin. Cancer Res. 10 (2004) 7365–7374. (c) G. Darnell, D. R. Richardson, Blood, 94 (1999) 781–792. (d) L. R. Morgan, B. S. Jursic, C. L. Hooper, D. M. Neumann, K. Thangaraj, B. LeBlanc, Bioorg. Med. Chem. Lett. 12 (2002) 3407–3411. (e) G. S. Hassan, H. H. Kadry, S. M. Abou-Seri, M. M. Ali, A. E. E. D. Mahmoud, Bioorg. Med. Chem., 19 (2011) 6808–6817.

[35] D. S. Raja, N. S. P. Bhuvanesh, K. Natarajan, J. Biol. Inorg. Chem. 17 (2012) 223–237.

[36] Y. C. Liu, Z. Y. Yang, Eur. J. Med. Chem. 44 (2009) 5080–5089.

[37] Y. C. Liu, Z. Y. Yang, J. Inorg. Biochem. 103 (2009) 1014–1022.

[38] (a) C. D. Fan, H. Su, J. Zhao, B. X. Zhao, S. L. Zhang, J. Y. Miao, Eur. J. Med. Chem. 45 (2010) 1438–1446. (b) M. V. Angelusiu, S. F. Barbuceanu, C. Draghici and G. L. Almajan, Eur. J. Med. Chem. 45 (2010) 2055–2062. (c) G. Kumar, S. Devi, R. Johari, D.

Kumar, Eur. J. Med. Chem. 52 (2012) 269–274. (d) D. S. Raja, E. Ramachandran, N. S. P. Bhuvanesh, K. Natarajan, Eur. J. Med. Chem. 64 (2013) 148–159. (e) P. P. Netalkar, S. P. Netalkar, S. Budagumpi, V. K. Revankar, Eur. J. Med. Chem. 79 (2014) 47–56.

[39] (a) S. Kumar, S. Bawa, H. Gupta, Mini Rev. Med. Chem. 9 (2009) 1648–1654. (b) S. Bawa, S. Kumar, S. Drabu, R. Kumar, J. Pharm. Bioallied Sci. 2 (2010) 64–71.

[40] (a) J. P. Michael, Natural Product Reports 19 (2002) 742–760. (b) J. P. Michael, Natural Product Reports 25 (2008) 166–187.

[41] O. Afzal, S. Kumar, M. R. Haider, M. R. Ali, R. Kumar, M. Jaggi, S. Bawa, Eur. J. Med. Chem. 97 (2015) 871–910.

[42] M. Balasubramanian, J. G. Keay, in: A. R. Katritzky, C.W. Rees, E. F. V. Scriven (Eds.), Comprehensive Heterocyclic Chemistry II, vol. 5, Pergamon Press, Oxford, UK, (1996) p. 245.

[43] R. A. Rowe, M. M. Jones, Inorg. Synth. 5 (1957) 113–116.

[44] M. C. Mandewale, B. R. Thorat, D. Shelke, R. Patil, R. Yamgar, Heterocycl. Lett. 5 (2015) 251–259.

[45] S. P. Dash, A. K. Panda, S. Dhaka, S. Pasayat, A. Biswas, M. R. Maurya, P. K. Majhi, A. Crochet, R. Dinda, Dalton Trans. 45 (2016) 18292–18307.

[46] Bruker (2007) APEX2 (Version 2.1-4), SAINT (version 7.34A), SADABS (version 2007/4), BrukerAXS Inc, Madison, Wisconsin, USA.

[47] (a) A. Altomare, C. Burla, M. Camalli, G. L. Cascarano, C. Giacovazzo, A. Guagliardi, A. G. G. Moliterni, G. Polidori, R. Spagna, J. Appl. Crystallogr. 32 (1999) 115–119. (b) A. Altomare, G. L. Cascarano, C. Giacovazzo, A. Guagliardi, J. Appl. Crystallogr. 26 (1993) 343–350.

[48] G. M. Sheldrick SHELXL-97, Program for the Refinement of Crystal Structures. University of Göttingen, Germany, (1997).

[49] S. Mackay, C. Edwards, A. Henderson, C. Gilmore, N. Stewart, K. Shankland, A. Donald MaXus: a computer program for the solution and refinement of crystal structures from diffraction data. University of Glasgow, Scotland, (1997).

[50] G. M. Sheldrick, Acta Crystallogr., Sect. A: Found. Crystallogr. 64 (2008) 112–122.

[51] (a) D. Waasmaier, A. Kirfel, Acta Crystallogr. A. 51 (1995) 416–431. (b) A. J. C. Wilson, ed. International Tables for Crystallography. Vol. C. 1992, Kluwer Academic Publishers: Dordrecht.

[52] L. J. Farrugia. Ortep-3 for Windows. Journal of J. Appl. Crystallogr. 30 (1997) 565–566.

[53] *WinEPR SimFonia, version 1.25*, Bruker Analytische Messtechnik GmbH, Karlshrue, 1996.

[54] G. Micera, E. Garribba, J. Comput. Chem. 32 (2011) 2822–2835.

[55] (a) D. N. Chasteen in Biological Magnetic Resonance, Vol. 3 (Eds.: L. J. J. Berliner, J. Reuben), Plenum Press, New York, 1981, 53. (b) T. S. Smith, R. LoBrutto, V. L. Pecoraro, Coord. Chem. Rev. 228 (2002) 1–18. (c) E. Garribba, E. Lodyga-Chruscinska, G. Micera, A. Panzanelli, D. Sanna, Eur. J. Inorg. Chem. (2005) 1369–1382.

[56] M. J. Frisch, G. W. Trucks, H. B. Schlegel, G. E. Scuseria, M. A. Robb, J. R. Cheeseman, G. Scalmani, V. Barone, B. Mennucci, G. A. Petersson, H. Nakatsuji, M. L. Caricato, H. P. Hratchian, A. F. Izmaylov, J. Bloino, G. Zheng, J. L. Sonnenberg, M. Hada, M. Ehara, K. Toyota, R. Fukuda, J. Hasegawa, M. Ishida, T. Nakajima, Y. Honda, O. Kitao, H. Nakai, T. Vreven, J. A. Montgomery, Jr., J. E. Peralta, F. Ogliaro, M. Bearpark, J. J. Heyd, E. Brothers, K. N. Kudin, V. N. Staroverov, T. Keith, R. Kobayashi, J. Normand, K. Raghavachari, A. Rendell, J. C. Burant, S. S. Iyengar, J. Tomasi, M. Cossi, N. Rega, J. M. Millam, M. Klene, J. E. Knox, J. B. Cross, V. Bakken, C. J. Adamo, J., R. Gomperts, R. E. Stratmann, O. Yazyev, A. J. Austin, R. Cammi, C. Pomelli, J. W. Ochterski, R. L. Martin, K. Morokuma, V. G. Zakrzewski, G. A. Voth, P.

Salvador, J. J. Dannenberg, S. Dapprich, A. D. Daniels, Ö. Farkas, J. B. Foresman, J. V. Ortiz, J. Cioslowski, D. J. Fox, Gaussian 09, revision C.01, Gaussian, Inc., Wallingford, CT, (2010).

[57] S. Grimme, J. Antony, S. Ehrlich, H. Krieg, J. Chem. Phys. 132 (2010) 154104/1–154104/19.

[58] A. V. Marenich, C. J. Cramer, D. G. Truhlar, J. Phys. Chem. B, 113 (2009) 6378–6396.

[59] (a) E. Lodyga-Chruscinska, D. Sanna, E. Garribba, G. Micera, Dalton Trans. (2008) 4903–4916. (b) G. Micera, E. Garribba, Eur. J. Inorg. Chem. (2010) 4697–4710. (c) G. Micera, E. Garribba, Eur. J. Inorg. Chem. (2011) 3768–3780. (d) G. Micera, E. Garribba, Int. J. Quantum Chem. 112 (2012) 2486–2498. (e) L. Pisano, K. Varnagy, S. Timari, K. Hegetschweiler, G. Micera, E. Garribba, Inorg. Chem. 52 (2013) 5260– 5272. (f) D. Sanna, K. Várnagy, N. Lihi, G. Micera, E. Garribba, Inorg. Chem. 52 (2013) 8202–8213. (g) S. Kundu, D. Mondal, K. Bhattacharya, A. Endo, D. Sanna, E. Garribba, M. Chaudhury, Inorg. Chem. 54 (2015) 6203–6215. (h) S. P. Dash, S. Majumder, A. Banerjee, M. F. N. N. Carvalho, P. Adão, J. C. Pessoa, K. Brzezinski, E. Garribba, H. Reuter, R. Dinda, Inorg. Chem. 55 (2016) 1165–1182.

[60] (a) D. Sanna, K. Varnágy, S. Timári, G. Micera, E. Garribba, Inorg. Chem. 50 (2011) 10328–10341. (b) D. Sanna, V. L. Pecoraro, G. Micera, E. Garribba, J. Biol. Inorg. Chem. 17 (2012) 773–790.

[61] F. Neese, ORCA - An Ab Initio, DFT and Semiempirical Program Package, Version 4.0, Max-Planck-Institute for Chemical Energy Conversion, Mülheim a. d. Ruhr, 2017.

[62] (a) S. Gorelsky, G. Micera, E. Garribba, Chem. Eur. J. 16 (2010) 8167–8180. (b) D. Sanna, G. Sciortino, V. Ugone, G. Micera, E. Garribba, Inorg. Chem. 55 (2016) 7373–7387.

[63] (a) S.A. Aboafia, S. a. Elsayed, A. K. A. El-Sayed, A. M. El-Hendawy, J. Mol. Struct. 1158 (2018) 39–50 (b) A. A. Schilt, R.C. Taylor, J. Inorg. Nucl. Chem. 9 (1959) 211–221 (c) S. P. Dash, S. Pasayat, S. Bhakat, H. R. Dash, S. Das, R. J. Butcher, R. Dinda, Polyhedron 31 (2012) 524–529.

[64] S. P. Dash, A. K. Panda, S. Pasayat, R. Dinda, A. Biswas, E. R. T. Tiekink, Y. P. Patil, M. Nethaji, W. Kaminsky, S. Mukhopadhyay, S. K. Bhutia, Dalton Trans. 43 (2014) 10139–10156.

[65] S. P. Dash, A. K. Panda, S. Pasayat, R. Dinda, A. Biswas, E. R. T. Tiekink, S. Mukhopadhyay, S. K. Bhutia, W. Kaminsky, E. Sinn, RSC Adv. 5 (2015) 51852–51867.

[66] S. P. Dash, S. Pasayat, S. Saswati, S. Roy, R. Dinda, E. R. T. Tiekink, S. Mukhopadhyay, S. K. Bhutia, M. R. Hardikar, B. Joshi, Y. P. Patil, M. Nethaji, Inorg. Chem. 52 (2013) 14096–14107.

[67] S. P. Dash, A. K. Panda, S. Pasayat, S. Majumder, A. Biswas, W. Kaminsky, S. Mukhopadhyay, S. K. Bhutia, R. Dinda, J. Inorg. Biochem. 144 (2015) 1–12.

[68] R. Dinda, P. K. Majhi, P. Sengupta, S. Pasayat, S. Ghosh, L. R. Falvello, T. C. W. Mak, Polyhedron 29 (2010) 248–253.

[69] S. P. Dash, S. Roy, M. Mohanty, M. F. N. N. Carvalho, M. L. Kuznetsov, J. C. Pessoa, A. Kumar, Y. P. Patil, A. Crochet, R. Dinda, Inorg. Chem. 55 (2016) 8407–8421.

[70] (a) R. Dinda, P. Sengupta, S. Ghosh, T. C. W. Mak, Inorg. Chem. 41 (2002) 1684–1688. (b) R. Dinda, P. Sengupta, M. Sutradhar, T. C. W. Mak, S. Ghosh, Inorg. Chem. 47 (2008) 5634–5640.

[71] P. Adão, J. C. Pessoa, R. T. Henriques, M. L. Kuznetsov, F. Avecilla, M. R. Maurya, U. Kumar, I. Correia, Inorg. Chem. 48 (2009) 3542–3561.

[72] P. K. Sasmal, A. K. Patra, A. R. Chakravarty, J. Inorg. Biochem. 102 (2008) 1463–1472.

[73] M. R. Nimlos, D. F. Kelley, E. R. Bernstein, J. Phys. Chem. 91 (1987) 6610–6614.

[74] S. Sklenák, Y. Apeloig, Z. Rappoport, J. Am. Chem. Soc. 120 (1998) 10359–10364.

[75] (a) A. Avdeef, Absorption and Drug Development: Solubility, Permeability, and Charge State, Second Edition, John Wiley & Sons, Inc, Hoboken, New Jersey, (2012). (b) A. Avdeef, Curr. Top. Med. Chem. 1 (2001) 277–351.

[76] D. Sanna, P. Buglyo, A. I. Tomaz, J. C. Pessoa, S. Borovic, G. Micera, E. Garribba, Dalton Trans. 41 (2012) 12824–12838.

[77] G. Sciortino, D. Sanna, V. Ugone, G. Micera, A. Lledós, J.-D. Maréchal, E. Garribba, Inorg. Chem. 56 (2017) 12938–12951.

[78] M. Wenzel, A. Casini, Coord. Chem. Rev. 352 (2017) 432–460.

[79] K. Strupat, Methods Enzymol. 405 (2005) 1–36.

[80] A. Casini, C. Gabbiani, G. Mastrobuoni, L. Messori, G. Moneti, G. Pieraccini, ChemMedChem. 1 (2006) 413–417.

[81] (a) D. Sanna, V. Ugone, G. Sciortino, P. Buglyo, Z. Bihari, P. L. Parajdi-Losonczi, E. Garribba, Dalton Trans. 47 (2018) 2164–2182. (b) G. Sciortino, D. Sanna, V. Ugone, A. Lledós, J.-D. Maréchal, E. Garribba, Inorg. Chem. 57 (2018) 4456–4469. (c) G. Sciortino, D. Sanna, V. Ugone, J.-D. Maréchal, E. Garribba, Inorg. Chem. Front. 6 (2019) 1561–1578. (d) V. Ugone, D. Sanna, G. Sciortino, J.-D. Maréchal, E. Garribba, Inorg. Chem. 58 (2019) 8064–8078. (e) G. Sciortino, D. Sanna, V. Ugone, J.-D. Maréchal, M. Alemany-Chavarria, E. Garribba, New J. Chem. DOI: 10.1039/c9nj01956a.

[82] (a) M. Das, R. Nasani, M. Saha, M. M. Shaikh, S. Mukhopadhyay, Dalton Trans. 44 (2015) 2299–2310. (b) M. Saha, M. Das, R. Nasani, I. Choudhuri, M. Yousufuddin, H. P. Nayek, M. M. Shaikh, B. Pathaka, S. Mukhopadhyay, Dalton Trans. 44 (2015) 20154–20167.

[83] E. Gao, L. Liu, M. Zhu, Y. Huang, F. Guan, X. Gao, M. Zhang, L. Wang, W. Zhang, Y. Sun, Inorg. Chem. 50 (2011) 4732–4741.

[84] P. J. Bindu, K. M. Mahadevan, T. R. R. Naik, B. G. Harish, Med. Chem. Commun. 5 (2014) 1708–1717.

[85] Y. Sun, Y.-J. Hou, Q.-X. Zhou, W.-H. Lei, J.-R. Chen, X.-S. Wang, B.-W. Zhang, Inorg. Chem. 49 (2010) 10108–10116.

[86] Z.-g. Wang, Y.-y. Kou, J. Lu, C.-y. Gao, J.-l. Tian, S.-p. Yan, Appl. Organomet. Chem. 26 (2012) 511–517.

Graphical Abstract (Figure)

Chemistry of mixed-ligand oxidovanadium(IV) complexes of aroylhydrazones incorporating quinoline derivatives: Study of solution behavior, theoretical evaluation and protein/DNA interaction

Atanu Banerjee, Subhashree P. Dash, Monalisa Mohanty, Daniele Sanna, Giuseppe Sciortino, Valeria Ugone, Eugenio Garribba,* Hans Reuter, Werner Kaminsky, Rupam Dinda*

Exploration of synthesis, structure, solution behavior, theoretical evaluation and protein/DNA interaction of mixed-ligand oxidovanadium(IV) [VO($\mathbf{L}^{x}$)($\mathbf{L}^{N\text{-}N}$)] (**1**-**8**) (Where $\mathbf{L}^{x}$ = four different ONO donor aroylhydrazon ligands, and $\mathbf{L}^{N\text{-}N}$ = *N*,*N*-donor bases like 2,2′-bipyridine (**1**, **3**, **5** and **7**) and 1,10-phenanthroline (**2**, **4**, **6** and **8**)) complexes of aroylhydrazones incorporating quinoline derivatives.

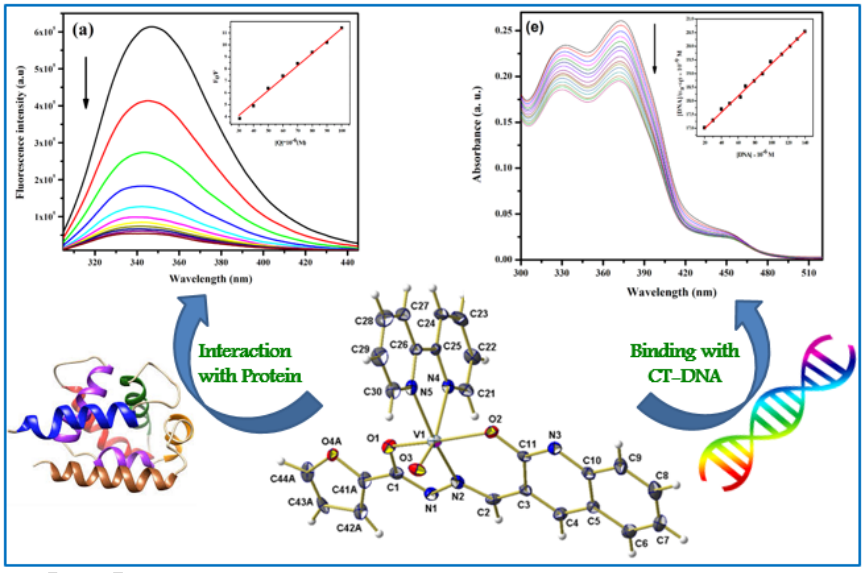

Graphical Abstract (Synopsis)

Chemistry of mixed-ligand oxidovanadium(IV) complexes of aroylhydrazones incorporating quinoline derivatives: Study of solution behavior, theoretical evaluation and protein/DNA interaction

Atanu Banerjee, Subhashree P. Dash, Monalisa Mohanty, Daniele Sanna, Giuseppe Sciortino, Valeria Ugone, Eugenio Garribba,* Hans Reuter, Werner Kaminsky, Rupam Dinda*

Exploration of synthesis, structure, solution behavior, theoretical evaluation and protein/DNA interaction of mixed-ligand oxidovanadium(IV) [VO($\mathbf{L}^{x}$)($\mathbf{L}^{N\text{-}N}$)] (**1**-**8**) (Where $\mathbf{L}^{x}$ = four different ONO donor aroylhydrazon ligands and $\mathbf{L}^{N\text{-}N}$ = *N*,*N*-donor bases like 2,2′-bipyridine (**1**, **3**, **5** and **7**) and 1,10-phenanthroline (**2**, **4**, **6** and **8**)) complexes of aroylhydrazones incorporating quinoline derivatives.

Research Highlights

Chemistry of mixed-ligand oxidovanadium(IV) complexes of aroylhydrazones incorporating quinoline derivatives: Study of solution behavior, theoretical evaluation and protein/DNA interaction

Atanu Banerjee, Subhashree P. Dash, Monalisa Mohanty, Daniele Sanna, Giuseppe Sciortino, Valeria Ugone, Eugenio Garribba,* Hans Reuter, Werner Kaminsky, Rupam Dinda*

- Aroylhydrazone ligands incorporating quinolone moiety
- Mixed-ligand oxidovanadium(IV) complexes
- Study of solution behavior
- Protein/DNA interaction.
- Theoretical evaluation